New Journal of Physics
The open-access journal for physics

Trapped Rydberg ions: from spin chains to fast quantum gates

Markus Müller[1,3], **Linmei Liang**[2], **Igor Lesanovsky**[1] **and Peter Zoller**[1]

[1] Institute for Theoretical Physics, University of Innsbruck, and Institute for Quantum Optics and Quantum Information of the Austrian Academy of Sciences, Innsbruck, Austria
[2] Department of Physics, National University of Defense Technology, Changsha 410073, People's Republic of China
E-mail: markus.mueller@uibk.ac.at

New Journal of Physics **10** (2008) 093009 (29pp)
Received 20 April 2008
Published 10 September 2008
Online at http://www.njp.org/
doi:10.1088/1367-2630/10/9/093009

Abstract. We study the dynamics of Rydberg ions trapped in a linear Paul trap, and discuss the properties of ionic Rydberg states in the presence of the static and time-dependent electric fields constituting the trap. The interactions in a system of many ions are investigated and coupled equations of the internal electronic states and the external oscillator modes of a linear ion chain are derived. We show that strong dipole–dipole interactions among the ions can be achieved by microwave dressing fields. Using low-angular momentum states with large quantum defect, the internal dynamics can be mapped onto an effective spin model of a pair of dressed Rydberg states that describes the dynamics of Rydberg excitations in the ion crystal. We demonstrate that excitation transfer through the ion chain can be achieved on a nanosecond timescale and discuss the implementation of a fast two-qubit gate in the ion chain.

[3] Author to whom any correspondence should be addressed.

Contents

1. Introduction

Rydberg states correspond to the infinite series of excited bound states in a Coulomb potential with large principal quantum number n. In view of their 'macroscopic' size, $a_{\mathrm{Ry}} \sim n^2 a_0$ with a_0 the atomic Bohr radius, Rydberg states have remarkable properties, as reflected, for example, in their response to external static and time-dependent electric and magnetic fields [1]. While the single particle physics of Rydberg atoms has been the subject of intensive studies in the context of laser spectroscopy, recent interest has focused on exploiting the large and long-range interactions between laser-excited Rydberg atoms to manipulate the many-body properties of cold atomic ensembles. Examples include recent seminal experiments on frozen Rydberg gases obtained by laser excitation from cold atomic gases, demonstrating in particular a dipole-blockade mechanism [2]–[7], which in sufficiently dense gases prevents the excitation of ground-state atoms in the vicinity of a Rydberg atom, and proposals for fast two-qubit quantum gates between pairs of atoms in optical lattices [8]. Furthermore, Rydberg atoms have been proposed to serve as model systems for studying coherent transport of excitations [9]—a mechanism that is of great importance for coherent energy transfer in biological systems, e.g. in light-harvesting complexes [10, 11]. While these investigations have so far concentrated on neutral atoms, we are interested below in describing the properties of laser-excited Rydberg ions stored in a Paul trap, in particular the interplay between trapping fields and Rydberg excitations, and the associated many-body interactions in a chain of cold trapped Rydberg ions.

Atomic ions can be stored in static and radiofrequency (RF) electric quadrupole fields constituting a Paul trap [12], where for sufficiently low temperature they form a Wigner

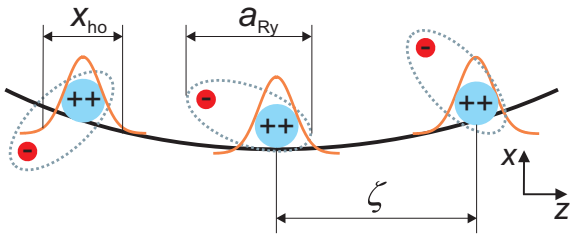

Figure 1. Typical length scales in a chain of cold Rydberg ions in a linear Paul trap. The external trapping frequency is in the order of megahertz (MHz) with a corresponding oscillator length x_{ho} of approximately 10 nm. The interparticle spacing ζ, set by the equilibrium between the Coulomb forces among the ions and the external confinement, is typically about 5 μm. The third length scale is the size of the Rydberg orbit a_{Ry}. Due to the scaling proportional to the square of the principal quantum number n it can assume values in the order of 100 nm and therefore become significantly larger than x_{ho}. In this regime the Rydberg ion cannot be considered as a point particle but rather as a composite object, and its internal structure must be taken into account.

crystal [13]–[17]. By using laser cooling, the ions can be prepared in the vibrational ground states of the phonon modes of the crystal. Internal electronic states of the ions can be manipulated with laser light and entangled via the collective phonon modes. Here we consider a situation where ions initially prepared in their electronic ground state are excited with laser light to high-lying Rydberg states. In contrast with ions in low-lying electronic states, a Rydberg ion in a Paul trap must be understood as a *composite object*, where the Rydberg electron is bound by the Coulomb force to the doubly charged ion core, but both the Rydberg electron and the ion core move in the electric fields constituting the trapping potentials. This is reminiscent of the situation in which Rydberg atoms are confined by very tight magnetic traps [18, 19]. We are particularly interested in the parameter regime where the size of the Rydberg orbit a_{Ry} is larger than the localization length of the doubly charged ion core x_{ho} around its equilibrium position, but still much smaller than the average distance ζ between the ions in the Wigner crystal, i.e. $x_{ho} < a_{Ry} \ll \zeta$ (see figure 1). Our goal is to provide a description of the interaction and quantum dynamics of such a one-dimensional (1D) string of Rydberg ions in a linear ion trap.

In comparison with neutral Rydberg atoms, a number of features and differences emerge for Rydberg ions in a Paul trap, which will be illuminated in the present work. First of all, the character of a Rydberg ion as a composite object gives rise to an intrinsic coupling of electronic and external motion in the presence of the electric trapping fields. This will be shown to result in renormalized trapping frequencies for Rydberg ions compared with their ground-state counterparts. Furthermore, the interaction among ions is not—as in the neutral case—governed by the dipole–dipole force alone but also by the charge-charge, dipole–charge and charge–quadrupole interaction. The interplay of this rich variety of interactions among the ions and the external trapping fields will be analyzed.

In our study we focus on ionic Rydberg states with low angular momentum quantum number and correspondingly large quantum defect, and large fine structure splitting, as these states can be most simply described and most easily excited by laser light from electronic ground states. For typical ion trap parameters [12], static dipolar and van der Waals interaction

among ions in these Rydberg states is shown to be small compared with the energy scale set by the external trapping frequencies of the ions. Thus, in order to establish substantially stronger interactions, we employ additional microwave (MW) fields driving transitions between Rydberg states. This leads to large oscillating dipole moments, which result in remarkably strong controllable dipole–dipole interactions between the ions. Our findings show that for strong interactions the internal and external dynamics of the ion chain approximately decouple such that a 'frozen' Rydberg gas is formed. In this limit the Hamiltonian describing the electronic dynamics can be formulated in an effective spin-$\frac{1}{2}$ representation and involves resonant and off-resonant dipole–dipole interaction terms with coupling strengths of the order of several hundred MHz. Based on this effective spin model, we demonstrate resonant excitation transfer on a nanosecond timescale from one end to the other of the ion chain. Moreover, we show that a two-qubit conditional phase gate between adjacent ions, based on the dipole–dipole interaction, can be realized on a timescale which is much shorter than both the external dynamics and the radiative lifetime of the Rydberg states involved.

This paper is organized as follows: in section 2, we derive the Hamiltonian of the coupled internal and external dynamics of a single Rydberg ion in a linear Paul trap. We analyze the effects of the trapping fields on the electronic properties of an ion excited to a Rydberg state, introduce MW-dressed Rydberg states and study the coupled electronic and external equations of motion within a Born–Oppenheimer approach. In section 3, we turn to the analysis of several trapped Rydberg ions, discuss the variety of interactions among the ions and derive the effective spin-$\frac{1}{2}$ Hamiltonian for the electronic dynamics in the ion chain. Finally, we illustrate the quantum dynamics of the system by studying resonant excitation transfer and present the fast two-qubit gate scheme.

2. A single trapped Rydberg atom as a composite object

2.1. Single Rydberg ion in a linear Paul trap

A combination of static and time-dependent electric fields can be employed to confine charged particles in a restricted region of space. The electric potential of a quadrupole field of a standard Paul trap can be written in the form

$$\Phi_T(\mathbf{r}, t) = \alpha \cos(\omega t)\left[x^2 - y^2\right] - \beta\left[x^2 + y^2 - 2z^2\right], \tag{1}$$

where ω is the RF drive frequency. The electric field gradients α and β are determined by the actual geometry of the experimental setup. In the present experiments, typical parameters are $\alpha \sim 10^9\,\mathrm{V\,m^{-2}}$, $\beta \sim 10^7\,\mathrm{V\,m^{-2}}$ and $\omega = 2\pi \times 10 \ldots 100\,\mathrm{MHz}$ (for details see e.g. [12]).

We are interested in the properties of Rydberg ions of alkali earth metals [20] in an electric quadrupole trap. They possess a single valence electron with the remaining electrons forming closed shells [1]. For the description of such a system, one can employ an effective two-body approach in which the ion is modeled by a two-fold positively charged core (mass M, position $\mathbf{r}_\mathrm{c}$) and the valence electron (mass m, position $\mathbf{r}_\mathrm{e}$). The corresponding interaction (model-)potential depends on the relative coordinate $\mathbf{r}_\mathrm{c} - \mathbf{r}_\mathrm{e}$ and also on the angular momentum state of the atom. The latter dependence accounts for the quantum defect—a lowering in the energy for low-angular-momentum states in which the valence electron probes the inner electronic shells. High-angular-momentum states (typically with angular momentum quantum number $l > 5$) do not exhibit a significant quantum defect since here the valence electron is located far away from the ionic core thus experiencing a bare Coulomb potential.

We now formulate the Hamiltonian of a single Rydberg ion in the presence of the electric potential of the Paul trap. We add a linear potential, corresponding to a time-dependent homogeneous electric field, $\Phi_l(\mathbf{r}) = \mathbf{f}(t)\cdot\mathbf{r}$, such that the combined electric potential reads $\Phi(\mathbf{r},t) = \Phi_T(\mathbf{r},t) + \Phi_l(\mathbf{r},t)$. Below, we will employ this additional MW field to electronically couple different Rydberg states. This will allow us to generate large oscillating dipole moments, which give rise to strong dipole–dipole interactions among dressed Rydberg ions.

Writing the interaction potential between the valence electron and the atomic core as $V(|\mathbf{r}_e - \mathbf{r}_c|)$ and taking into account the coupling of the individual charges to the electric potentials, we find

$$H_{\text{lab}} = \frac{\mathbf{p}_c^2}{2M} + \frac{\mathbf{p}_e^2}{2m} + V(|\mathbf{r}_e - \mathbf{r}_c|) + 2e\Phi(\mathbf{r}_c,t) - e\Phi(\mathbf{r}_e,t) + H_{\text{FS}}. \tag{2}$$

The term H_{FS} accounts for the spin–orbit coupling giving rise to the fine structure of electronic levels. Its effect will be discussed in the following subsection.

We introduce center of mass (CM) $\mathbf{R} = (X, Y, Z)$ and relative coordinates $\mathbf{r} = (x, y, z)$ according to

$$\mathbf{r}_c = \mathbf{R} - \frac{m}{M+m}\mathbf{r}, \qquad \mathbf{r}_e = \mathbf{R} + \frac{M}{M+m}\mathbf{r}. \tag{3}$$

Exploiting that the nuclear mass is much larger than the electronic one and hence $M \gg m$, we have $\mathbf{r}_c \approx \mathbf{R}$ and $\mathbf{r}_e \approx \mathbf{R} + \mathbf{r}$. Within this approximation the Hamiltonian becomes

$$\begin{aligned} H &= \frac{\mathbf{P}^2}{2M} + \frac{\mathbf{p}^2}{2m} + V(|\mathbf{r}|) + 2e\Phi(\mathbf{R},t) - e\Phi(\mathbf{R}+\mathbf{r},t) + H_{\text{FS}} \\ &= \frac{\mathbf{P}^2}{2M} + \frac{\mathbf{p}^2}{2m} + V(|\mathbf{r}|) \\ &\quad + e\left[\Phi(\mathbf{R},t) - \frac{\partial\Phi(\mathbf{R},t)}{\partial\mathbf{R}}\cdot\mathbf{r} - \frac{1}{2}\sum_{kl} x_k \frac{\partial^2\Phi(\mathbf{R},t)}{\partial X_k \partial X_l} x_l\right] + H_{\text{FS}}. \end{aligned} \tag{4}$$

Corrections to this Hamiltonian scale with m/M, which is typically about 10^{-5}.

In the case of ions in low-lying electronic states, the potential (1) provides *static* confinement along the longitudinal (z-)direction. However, transversally at no instant of time is a confining potential present. One rather finds a periodically oscillating potential saddle centered at the origin of the coordinate system. Owing to the rapid periodic change of the confining and non-confining direction, however, the ions experience a ponderomotive potential that can provide transversal confinement [21]. In order to make this manifest, we transform into a frame which oscillates at the RF frequency ω in the CM coordinate system. This is achieved by the unitary transformation

$$U = U(\mathbf{R},t) = \exp\left(-\mathrm{i}\frac{e\alpha}{\hbar\omega}\left[X^2 - Y^2\right]\sin(\omega t)\right). \tag{5}$$

By applying this transformation to Hamiltonian (5), one obtains

$$H' = UHU^\dagger + \mathrm{i}\hbar\frac{\partial U}{\partial t}U^\dagger = H_{\text{CM}} + H_{\text{el}} + H_{\text{CM-el}} + H_{\text{mm}} \tag{6}$$

with

$$H_{\text{CM}} = \frac{\mathbf{P}^2}{2M} + \frac{1}{2}M\omega_z^2 Z^2 + \frac{1}{2}M\omega_\rho^2\left(X^2 + Y^2\right), \tag{7}$$

$$H_{\rm el} = \frac{\mathbf{p}^2}{2\,m} + V\,(|\mathbf{r}|) - e\Phi(\mathbf{r},t) + H_{\rm FS}, \tag{8}$$

$$H_{\rm CM-el} = -2e\left[\alpha\cos(\omega t)\,(Xx - Yy) - \beta\,(Xx + Yy - 2Zz)\right], \tag{9}$$

$$H_{\rm mm} = -\frac{2e\alpha}{M\omega}\sin(\omega t)\big(XP_x - YP_y\big) - \frac{e^2\alpha^2}{M\omega^2}(X^2+Y^2)\cos(2\omega t) + e\mathbf{f}(t)\cdot\mathbf{R}. \tag{10}$$

Here, $H_{\rm CM}$ provides harmonic axial and transversal confinement of the CM motion with the corresponding trap frequencies $\omega_z = 2\sqrt{\frac{e\beta}{M}}$ and $\omega_\rho = \sqrt{2}\sqrt{\left(\frac{e\alpha}{M\omega}\right)^2 - \frac{e\beta}{M}}$, which are of the order of a few MHz and satisfy $\omega_\rho \gg \omega_z$. For Ca^+ ions, an RF frequency $\omega = 2\pi \times 15\,\mathrm{MHz}$ and the gradient parameters $\alpha = 10^9\,\mathrm{V\,m^{-2}}$ and $\beta = 10^7\,\mathrm{V\,m^{-2}}$, the axial and radial trap frequencies evaluate to $\omega_z = 2\pi \times 1.56\,\mathrm{MHz}$ and $\omega_\rho = 2\pi \times 5.64\,\mathrm{MHz}$, respectively.

The term $H_{\rm el}$ contains all dependencies on the electronic coordinates describing the motion of an electron in the field of a doubly charged ionic core which is superimposed by the electric potential $\Phi(\mathbf{r},t)$. The electronic dynamics takes place on a much faster timescale compared with the CM motion in the trap. The external electric field prevents, unlike in the field-free case, the separation of the CM and relative dynamics. The coupling between these motions is accounted for by $H_{\rm CM-el}$. Owing to the large separation of timescales of electronic and external dynamics, we will treat this coupling within a Born–Oppenheimer approach below.

Finally, we have the term $H_{\rm mm}$, which gives rise to the micromotion causing a coupling between the static oscillator levels of $H_{\rm CM}$. It can be shown [21] that for large enough values of the RF frequency ω, this coupling can be neglected and the external motion of the ions can be considered as if it was taking place in a static harmonic potential. The effect of the additional micromotion term $e\mathbf{f}(t)\cdot\mathbf{R}$ arising from the MW dressing fields can likewise be neglected in the following, since typical MW frequencies are of the order of at least one gigahertz (GHz) and therefore far from being resonant with the external trapping frequency of the ions.

With the full Hamiltonian (6) for the internal and external dynamics and the coupling among them at hand, we are now in a position to analyze the electronic properties of a trapped Rydberg ion and the mutual interplay of internal and external dynamics. This will be addressed in the next two subsections.

2.2. Electronic properties

We proceed by inspecting the electronic Hamiltonian $H_{\rm el}$ in (8),

$$H_{\rm el} = \frac{\mathbf{p}^2}{2\,m} + V\,(|\mathbf{r}|) + H_{\rm FS} + H_{\rm ef} \tag{11}$$

with the electric trapping and MW dressing fields contained in

$$\begin{aligned} H_{\rm ef} &= -e\Phi(\mathbf{r},t) = H_{\rm stat} + H_{\rm osc} + H_{\rm MW} \\ &= e\,\beta\left[x^2 + y^2 - 2z^2\right] - e\,\alpha\cos(\omega t)\left[x^2 - y^2\right] - e\,\mathbf{f}(t)\cdot\mathbf{r}. \end{aligned} \tag{12}$$

In the absence of electric fields the ionic Rydberg states can be classified by the principal quantum number n, the angular momentum quantum number l, the total angular momentum j and its magnetic quantum number m. The quantum states are represented by $|n,l,j,m\rangle = |n,l\rangle|j,m\rangle_a$, which factors in the radial part $|n,l\rangle$ and the angular momentum part $|j,m\rangle_a$. The latter is constituted by a linear combination of products of the spherical harmonics and spin orbitals. The corresponding energies of the Rydberg levels are given by the well-known formula

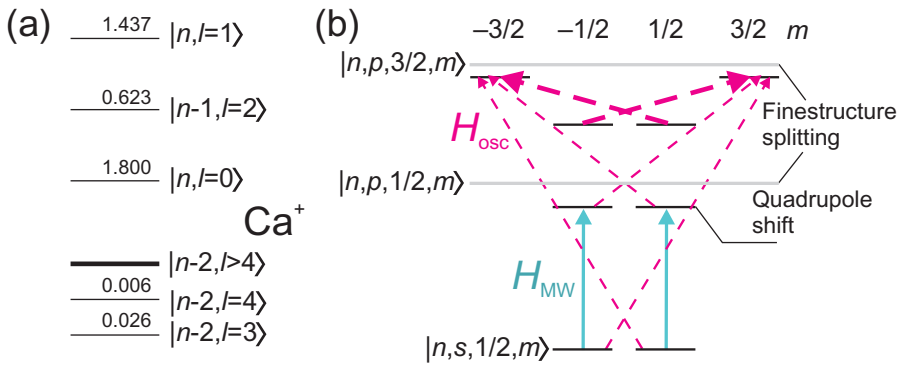

Figure 2. (a) Sketch of the Rydberg level structure of the Ca^+ ion in the field-free case without fine structure. States with $l > 4$ do not exhibit a quantum defect and are located in a degenerate manifold of states. States with low angular momentum are split away from this manifold. The corresponding quantum defects are provided (taken from [20]). (b) Levels of the s and p manifold in the presence of the electric potential $\Phi(\mathbf{r}, t)$. Its static components lead to a first-order shift (quadrupole shift) of the energy levels according to (13) and (14). In general the electronic energy is lowered with respect to the field-free value (sketched by the solid gray lines). The shifted levels are coupled by the MW Hamiltonian H_{MW} (blue, solid lines) and the oscillating components of the trapping field (red, dashed lines). We consider that the limit of large fine structure splitting in which the coupling between the states $|n, \mathrm{p}, 1/2, m\rangle$ and $|n, \mathrm{p}, 3/2, m\rangle$ (thin dashed lines), which is caused by H_{osc}, can be neglected.

$E_{n\,l\,j} = -4\,E_{\mathrm{Ryd}}/(n - \delta(l))^2 + E_{\mathrm{FS}}(n, l, j)$, where $E_{\mathrm{Ryd}} = 13.6\,\mathrm{eV}$ is the Rydberg constant and $\delta(l)$ the quantum defect [1, 20]. The energy $E_{\mathrm{FS}}(n, l, j)$ accounts for the fine structure splitting due to H_{FS}. The typical Rydberg level structure (without fine structure) is sketched in figure 2(a) for the case of Ca^+.

In this paper, we focus on states with large quantum defect, i.e. s and p states. This is motivated by the fact that these states are most easily accessible via laser excitations from the electronic ground states, and that they are energetically far separated from the degenerate manifold of states of higher angular momentum states. Generically, the energy separation $\triangle E_{l,l+1}$ between these states scales as n^{-3} for large n. In the case of Ca^+, the energy separation between the s and the p level is $\triangle E_{\mathrm{s,p}}/\hbar \sim 280\,\mathrm{GHz}$ for $n = 60$.

Let us now inspect the effect of the electron field interaction H_{ef} contained in the electronic Hamiltonian (12). We assume that the fine structure splitting of the p state is sufficiently large such that neither the oscillating nor the static part of H_{ef} cause significant coupling between the states $|n, \mathrm{p}, 1/2, m\rangle$ and $|n, \mathrm{p}, 3/2, m\rangle$ and j remains a good quantum number. Since the fine structure splitting scales proportionally to n^{-3} and becomes larger with increasing atomic mass, the validity of this assumption can be ensured either by choosing not too high principal quantum numbers or by employing heavy ions. Moreover, we can neglect the coupling between the s and p states, which is justified by their typical energy splitting of several 100 GHz. Considering first the static part H_{stat} of (12), we find that it gives rise to the following quadrupole shifts, which depend on j and m:

$$\triangle E_{\mathrm{s}} = 0, \tag{13}$$

$$\triangle E_{\mathrm{p}j|m|} = \frac{2}{15} e\beta \langle n, \mathrm{p} \mid r^2 \mid n, \mathrm{p} \rangle \left[2|m| - j - \frac{9}{2} \right]. \tag{14}$$

Here, $\langle n, l|r^2|n, l\rangle$ denotes the radial matrix element of r^2 calculated using the radial eigenfunctions that belong to the atomic interaction potential $V(|\mathbf{r}|)$. The total energy of the electronic states is hence given by $E_{nljm} = E_{nlj} + \triangle E_{lj|m|}$. The quadrupole shifts with respect to the unperturbed energy of the p states are sketched in figure 2(b).

Let us now turn to the oscillating part of the electric field, which is accounted for by the term H_{osc} in the Hamiltonian (12). Since the oscillation frequency ω is typically $2\pi \times 10 \ldots 100$ MHz, it is not sufficient to yield a resonant coupling between the s and the p states or between the fine structure components of the p manifold. However, by estimating $|\langle n, \mathrm{p}|r^2|n, \mathrm{p}\rangle| \approx a_0^2 n^4$, where a_0 is Bohr's radius, we find that $\langle H_{\mathrm{osc}}\rangle \approx e\,\alpha\, a_0^2 n^4 \cos(\omega t)$ and, hence, although no resonant coupling is present, the strong modulation amplitude, which grows proportional to the fourth power of the principal quantum number n, might give rise to significant level shifts. From the symmetry properties of H_{osc}, one concludes that only levels whose magnetic quantum number m differs by 2 are coupled. These couplings are indicated in figure 2(b) by the red, dashed arrows. Since we assume that the fine structure splitting is much larger than $|\langle H_{\mathrm{osc}}\rangle|_{\max}$ the $j = 1/2$ states are unaffected by H_{osc}. By contrast strong effects are to be expected in the $j = 3/2$ manifold. However, in what follows we will exclusively work with the Rydberg states $|n, \mathrm{s}\rangle \equiv |n, \mathrm{s}, 1/2, m\rangle$ and $|n, \mathrm{p}\rangle \equiv |n, \mathrm{p}, 1/2, m\rangle$ (see figure 2).

For too strong electric field gradients and too strong MW dressing fields, unwanted transitions from the $|n, \mathrm{s}\rangle$, $|n, \mathrm{p}\rangle$ states of interest to other Rydberg states might take place, and there is also the danger of ionizing the ion due to the static and time-dependent terms in the Hamiltonian (12). In appendix B, we show that up to principal quantum numbers around $n = 50$ for typical trapping fields [12] and the MW dressing field strengths we consider in this work, these effects are negligible.

Finally, the term H_{MW} in (12), which accounts for the additional MW dressing fields, is to be discussed. This will be the subject of the following subsection.

2.3. MW dressing of Rydberg levels

In this section, we describe how MW dressing fields can be employed to generate strong interactions in an ion chain. As will be shown in section 3.1 Rydberg ions aligned in a Wigner crystal in the Paul trap do not exhibit *permanent* dipole moments, and residual van der Waals interactions are small. Thus, our aim is to generate strong interactions using (near-)resonant MW dressing fields to couple electronic s and p Rydberg states as indicated in figure 2(b). We show in the following that the MW dressing gives rise to large *oscillating* dipole moments, which in turn lead to strong dipole–dipole interaction between Rydberg ions.

The energy separation between s and p Rydberg states belonging to the same principal quantum number and thus also the typical frequencies of the MW dressing fields are in the order of a few hundred GHz (cf section 2.2). Since the trapping frequencies determining the external motion of the ions are in the MHz range (cf section 2.1), coupling to the external motion is negligible and the MW fields exclusively affect the electronic degrees of freedom. Ideas similar to the MW dressing scheme described below were applied in the context of cold polar molecules, where a combination of static electric and MW fields was used in order to tune intermolecular two- and three-body interactions [22].

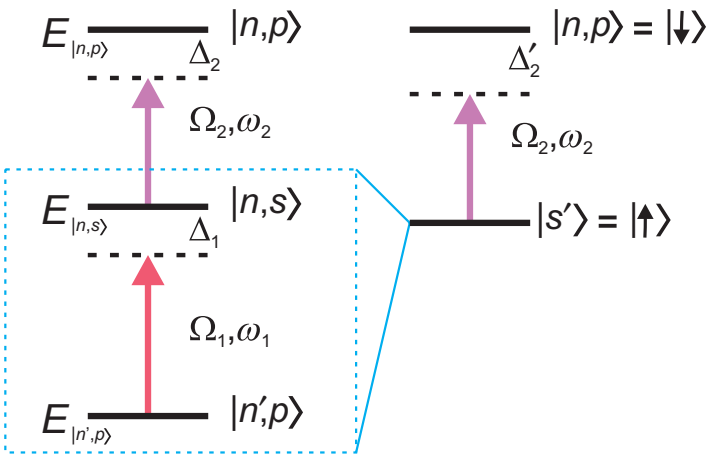

Figure 3. MW dressing of ionic Rydberg states. A linearly polarized bichromatic MW field is used to couple one s with two p levels one of which is far detuned. After an adiabatic elimination of the latter, one obtains an effective two-level system. This dressing is used to tailor the interaction between Rydberg ions.

In our setup we apply a linearly polarized MW such that non-zero transition dipole matrix elements occur between the states $|n, \mathrm{s}\rangle$ and $|n', \mathrm{p}\rangle$. For our purposes we choose a bichromatic MW field of the form $\mathbf{f}(t) = E_1\,\mathbf{e}_z \cos\omega_1 t + E_2\,\mathbf{e}_z \cos\omega_2 t$ such that the coupling Hamiltonian reads

$$H_{\mathrm{MW}} = -d_z\,[E_1 \cos\omega_1 t + E_2 \cos\omega_2 t]\,, \tag{15}$$

where $d_z = e\,z$ is the operator of the dipole moment. We consider three levels (one s level and two p levels), which are coupled by H_{MW} as depicted in figure 3. The frequencies ω_1 and ω_2 bridge the energy separations $E_{|n,\mathrm{s}\rangle} - E_{|n',\mathrm{p}\rangle}$ and $E_{|n,\mathrm{p}\rangle} - E_{|n,\mathrm{s}\rangle}$, respectively, and are assumed to differ significantly. This can be achieved by choosing not too close values of n and n'. In the rotating frame and after performing the rotating wave approximation, the electronic Hamiltonian of a single ion reads

$$\begin{aligned} H_{3\,\mathrm{levels}} = {} & \hbar\Delta_1 |n', \mathrm{p}\rangle\langle n', \mathrm{p}| - \hbar\Delta_2 |n, \mathrm{p}\rangle\langle n, \mathrm{p}| \\ & + \tfrac{1}{2}\left[\left(\hbar\Omega_1 |n, \mathrm{s}\rangle\langle n', \mathrm{p}| + \hbar\Omega_2 |n, \mathrm{p}\rangle\langle n, \mathrm{s}|\right) + \mathrm{h.c.}\right]. \end{aligned} \tag{16}$$

Here, we have introduced the MW detunings $\Delta_1 = \omega_1 - (E_{|n,\mathrm{s}\rangle} - E_{|n',\mathrm{p}\rangle})/\hbar$ and $\Delta_2 = \omega_2 - (E_{|n,\mathrm{p}\rangle} - E_{|n,\mathrm{s}\rangle})/\hbar$ and the Rabi frequencies $\Omega_{1,2} = -d_{1,2}E_{1,2}/3$, which involve the radial dipole matrix elements $d_1 = e\langle n, \mathrm{s}|r|n', \mathrm{p}\rangle$ and $d_2 = e\langle n, \mathrm{s}|r|n, \mathrm{p}\rangle$. We assume that the MW field with frequency ω_1 is far-detuned and only weakly couples the states $|n', \mathrm{p}\rangle$ and $|n, \mathrm{s}\rangle$. Furthermore, it is assumed that $|\Delta_1| \gg |\Omega_2|, |\Delta_2|$. Under the condition $\Omega_1 \ll |\Delta_1|$ we can adiabatically eliminate the $|n', \mathrm{p}\rangle$ state and obtain an effective two-level system consisting of the $|n, \mathrm{p}\rangle$ state and a dressed state (see also figure 3)

$$|\mathrm{s}'\rangle = |n, \mathrm{s}\rangle - \frac{\Omega_1}{2\Delta_1}|n', \mathrm{p}\rangle \tag{17}$$

with $\eta = \Omega_1/(2\Delta_1)$, $\eta \ll 1$. This effective two-level system can be mapped onto a spin-$\frac{1}{2}$ particle by identifying the states $|\mathrm{s}'\rangle$ and $|n, \mathrm{p}\rangle$ as eigenstates of the spin operator S_z with positive

(negative) eigenvalue. The Hamiltonian (16) then reduces to

$$H_0 = \frac{\hbar}{2}\begin{pmatrix} \Delta_2' & \Omega_2 \\ \Omega_2 & -\Delta_2' \end{pmatrix} \equiv \mathbf{hS} \tag{18}$$

with an effective magnetic field $\mathbf{h} = (\Omega_2, 0, \Delta_2')$, detuning $\Delta_2' = \triangle_2 - \Omega_1^2/(4\triangle_1)$ and the spin operator $\mathbf{S} = (S_x, S_y, S_z)$.

Owing to the weak admixture of the state $|n', \mathrm{p}\rangle$, the dressed state $|\mathrm{s}'\rangle$ obtains an oscillating dipole moment. The matrix representation of the dipole operator d_z in the set of states $|\mathrm{s}'\rangle$, $|n, \mathrm{p}\rangle$ is given by

$$d_z = \frac{1}{3}\begin{pmatrix} -\frac{\Omega_1}{\Delta_1} d_1 \cos\omega_1 t & d_2 \mathrm{e}^{-\mathrm{i}\omega_2 t} \\ d_2 \mathrm{e}^{\mathrm{i}\omega_2 t} & 0 \end{pmatrix}. \tag{19}$$

Using the abbreviation $D_{1,2} = (d_{1,2}/3)^2$, one obtains the following representation of the dipole moment operator:

$$d_z = -\eta\sqrt{D_1}\cos(\omega_1 t)(1 + 2S_z) + 2\sqrt{D_2}(\cos(\omega_2 t)S_x + \sin(\omega_2 t)S_y). \tag{20}$$

The magnitude of the induced dipole moments is determined by the transition dipole matrix elements $d_{1,2}$, which can be roughly estimated as $d_{1,2} \sim ea_0 n^2$. Thus the dipole–dipole interaction energy scales $\sim n^4$ for large n. This is to be compared with the radiative lifetime of Rydberg states, which for large n and low l scales according to $\sim n^3$ [1], thereby favoring larger values of n. We return to the question of radiative decay and the validity of our analysis in section 3.2, where we will use the representation (20) of the dipole moment operator to derive an effective spin chain Hamiltonian describing the dynamics of Rydberg excitations in the ion chain.

2.4. Coupling between internal and external dynamics

In this section, we will analyze the effects of the coupling of internal and external degrees of freedom described by $H_{\mathrm{CM-el}}$ in the Hamiltonian (6). We treat these coupling terms using a Born–Oppenheimer approach, which is reasonable since the electronic dynamics takes place on a much faster timescale than the external motion of the ions. In this framework, we treat the CM coordinates as parameters while diagonalizing the electronic Hamiltonian. We evaluate the energy of the $|n, \mathrm{s}\rangle$-level by second-order perturbation theory considering only the coupling to the next $|n, \mathrm{p}\rangle$-level. After averaging over one RF cycle one obtains the energy correction

$$\epsilon(X, Y, Z) = E_{|n,\mathrm{s}\rangle} + \tfrac{1}{2}M\omega_z'^2 Z^2 + \tfrac{1}{2}M\omega_\rho'^2 (X^2 + Y^2) \tag{21}$$

with

$$\omega_z'^2 = -\frac{32}{3M}\frac{e^2\beta^2}{\triangle E_{\mathrm{s,p}}}|\langle n, \mathrm{s}|r|n, \mathrm{p}\rangle|^2, \tag{22}$$

$$\omega_\rho'^2 = -\frac{2}{3M}\frac{e^2(\alpha^2 + 2\beta^2)}{\triangle E_{\mathrm{s,p}}}|\langle n, \mathrm{s}|r|\, n, \mathrm{p}\rangle|^2, \tag{23}$$

and the energy difference $\triangle E_{\mathrm{s,p}} = E_{|n,\mathrm{p}\rangle} - E_{|n,\mathrm{s}\rangle}$. Hence, ions excited to Rydberg states experience modified transversal and longitudinal trap frequencies in comparison with their ground-state counterparts. For the s state under consideration the trap becomes shallower and

the new trap frequencies are given by $\tilde{\omega}_{\rho,z} = \omega_{\rho,z}\sqrt{1+(\omega'_{\rho,z}/\omega_{\rho,z})^2} \approx \omega_{\rho,z} + \omega'^2_{\rho,z}/(2\omega_{\rho,z}) = \omega_{\rho,z} + \delta\omega_{\rho,z}$, yielding

$$\frac{\delta\omega_z}{\omega_z} = \frac{4}{3}e\beta\frac{|\langle n,\mathrm{s}\,|r\,|n,\mathrm{p}\rangle_r|^2}{\triangle E_{\mathrm{s,p}}}, \tag{24}$$

$$\frac{\delta\omega_\rho}{\omega_\rho} = \frac{1}{6}\frac{\alpha^2+2\beta^2}{\alpha^2/(M\omega^2)-\beta/e}\frac{|\langle n,\mathrm{s}|r\,|n,\mathrm{p}\rangle_r|^2}{\triangle E_{\mathrm{s,p}}}. \tag{25}$$

By estimating $|\langle n,\mathrm{s}|r|n,\mathrm{p}\rangle| \sim a_0 n^2$, one finds that the frequency shift $\delta\omega_{\rho,z}$ scales proportional to n^7. For typical trap parameters, i.e. $\alpha \gg \beta$, the modification of the axial trap frequency is much smaller than the corresponding one for the radial frequency. For $n = 50$ and the parameters presented in section 2.2, we find $(\delta\omega_\rho)/\omega_\rho = 3.5\times10^{-2}$ and $(\delta\omega_z)/\omega_z = 7.4\times10^{-4}$. Below we are interested in the regime where these modifications of the trapping frequencies are negligible. We remark, though, that owing to the scaling $\sim n^7$ they can become significant even for moderately larger principal quantum numbers. These shifts of the external trapping frequencies might serve as an experimental signature of the successful preparation of single-ion Rydberg states[4].

3. Interacting trapped Rydberg ions

We now turn to the discussion of the interaction between several ions. First, we analyze the various types of emerging interactions between Rydberg ions, and discuss the interplay of interionic interactions and the effect of the external trapping fields. Then we proceed with the discussion of interacting Rydberg ions dressed by MW fields and derive the corresponding effective spin-$\frac{1}{2}$ Hamiltonian describing the Rydberg excitation dynamics in the ion chain. The role of the two effective spin states of each ion will be played by two Rydberg states, as outlined in section 2.3 and illustrated in figure 3.

We illustrate the effective spin dynamics by studying the process of resonant excitation transfer in a chain of ten ions. Furthermore, we suggest a scheme which allows us to observe the effective spin dynamics in dressed ground-state ions. We finally show how the trapped Rydberg ion system can be exploited in the context of quantum information processing and discuss an implementation of a two-qubit conditional phase gate.

3.1. Static interactions between trapped Rydberg ions

We consider the interaction between ions i and j with coordinates given by $(\mathbf{R}_i, \mathbf{r}_i)$ and $(\mathbf{R}_j, \mathbf{r}_j)$ as depicted in figure 4. The Coulomb interaction $V(\mathbf{r}_i, \mathbf{r}_j, \mathbf{R}_i, \mathbf{R}_j)$ between the charges belonging to different ions can be written as

$$\frac{V(\mathbf{R}_i,\mathbf{R}_j,\mathbf{r}_i,\mathbf{r}_j)}{e^2/(4\pi\epsilon_0)} = \frac{4}{|\mathbf{R}_i-\mathbf{R}_j|} - \frac{2}{|\mathbf{R}_i-(\mathbf{R}_j+\mathbf{r}_j)|} - \frac{2}{|(\mathbf{R}_i+\mathbf{r}_i)-\mathbf{R}_j|} + \frac{1}{|(\mathbf{R}_i+\mathbf{r}_i)-(\mathbf{R}_j+\mathbf{r}_j)|}. \tag{26}$$

[4] They could e.g. be measured by a spin-echo technique, which has been recently demonstrated in a two-ion experiment on nonlinear coupling of vibrational modes [23].

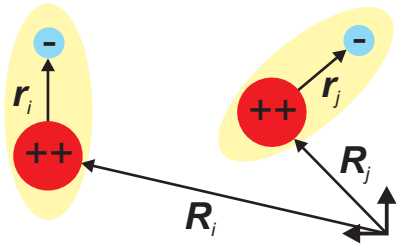

Figure 4. Interacting Rydberg ions. The net charge of the ions leads, apart from the common Coulomb repulsion, to a charge–dipole and a charge–quadrupole interaction both of which are absent in systems of neutral Rydberg atoms.

We assume that $|\mathbf{R}_i - \mathbf{R}_j| \gg |\mathbf{r}_{i/j}|$, which is very well fulfilled, since—as discussed above—we are interested in the parameter regime where the average interparticle distance ζ in the ion trap is much larger than the extension of the electronic wavefunction a_{Ry} of the Rydberg ions. Performing a multipole expansion up to second order in the small parameter (a_{Ry}/ζ) and abbreviating $|\mathbf{R}_i - \mathbf{R}_j| = |\mathbf{R}_{ij}| = R_{ij}$ and $\mathbf{n}_{ij} = (\mathbf{R}_i - \mathbf{R}_j)/R_{ij}$, we obtain the following form for the Rydberg ion–Rydberg ion interaction potential:

$$\frac{V(\mathbf{R}_i, \mathbf{R}_j, \mathbf{r}_i, \mathbf{r}_j)}{e^2/(4\pi\epsilon_0)} = \frac{1}{R_{ij}} + \frac{(\mathbf{R}_i - \mathbf{R}_j)(\mathbf{r}_i - \mathbf{r}_j)}{R_{ij}^3} + \frac{r_i^2 - 3(\mathbf{n}_{ij}\cdot\mathbf{r}_i)^2 + r_j^2 - 3(\mathbf{n}_{ij}\cdot\mathbf{r}_j)^2}{2R_{ij}^3} + \frac{\mathbf{r}_i\cdot\mathbf{r}_j - 3(\mathbf{n}_{ij}\cdot\mathbf{r}_i)(\mathbf{n}_{ij}\cdot\mathbf{r}_j)}{R_{ij}^3}. \tag{27}$$

The first term accounts for the Coulomb interaction between two singly charged ions and is independent of the degree of electronic excitation. In the case of Rydberg ions, the displacement of the electronic charge from the ionic core leads to the exhibition of a dipole moment which interacts with the charge of the other ion. This dipole–charge interaction gives rise to the second term. The third term accounts for the charge–quadrupole interaction. These three terms are absent in the case of interacting neutral Rydberg atoms. The last term is the well-known dipole–dipole interaction, which is also present in neutral systems.

For N ions stored in a Paul trap, at sufficiently low temperature and tight radial trapping, $\omega_\rho \gg \omega_z$, the ions form a 1D Wigner crystal with equilibrium positions along the Z-axis [15, 16], which are determined by the interplay between the Coulomb repulsion among the ions and the external confinement by the trapping fields. In appendix C, we show that after a harmonic expansion of the Hamiltonian around the equilibrium positions $Z_i^{(0)}$ (given by (C.3)), the full Hamiltonian of N interacting ions can be written as

$$H_{\mathrm{ions}} = H_{\mathrm{ph}} + \sum_i^N H_{\mathrm{el},i} + H_{\mathrm{int-ext}} + H_{\mathrm{dd}}. \tag{28}$$

The first term

$$H_{\mathrm{ph}} = \sum_{\alpha=x,y,z}\sum_n^N \hbar\omega_{\alpha,n} a_{\alpha,n}^\dagger a_{\alpha,n} \tag{29}$$

describes the external oscillation dynamics of the ionic cores with $a_{\alpha,n}^\dagger$ and $a_{\alpha,n}$ being the respective creation and annihilation operators of the normal modes (cf (C.5)–(C.8)). The second

term determines the electronic level structure of the ions: the charge–quadrupole term gives rise to a position-dependent variation of the electric field experienced by the trapped ions, which can be absorbed in the single-particle ion–field interaction $H_{\rm ef}$ given by (12). Thus, the electronic Hamiltonian of the ith ion takes the form

$$H_{\rm el,i} = \frac{\mathbf{p}_i^2}{2\,m} + V\,(|\mathbf{r}_i|) + e\,\beta_i'\left[x_i^2 + y_i^2 - 2z_i^2\right] - e\,\alpha\cos(\omega t)\left[x_i^2 - y_i^2\right] - e\,\mathbf{f}(t)\cdot\mathbf{r}_i \tag{30}$$

with position-dependent gradient

$$\beta_i' = \beta + \frac{e}{8\pi\epsilon_0}\sum_{j(\neq i)}^{N}\frac{1}{|Z_i^{(0)} - Z_j^{(0)}|^3} = \beta + \delta\beta_i. \tag{31}$$

The third term $H_{\rm int-ext}$ in (28) accounts for the coupling of the internal and external dynamics, which is partly due to the dipole–charge interaction and partly due to the inhomogeneous electric field of the Paul trap (see (C.12)). The resulting coupling between the internal and external dynamics becomes also position-dependent and thus leads to a state-dependent variation of the trapping frequency (see section 2.4). However, since we work in a regime where these shifts are negligible already in the single-ion case, they can also be neglected in the case of many ions.

Finally, we have the dipole–dipole interaction in (28), which after the harmonic expansion is given by

$$H_{\rm dd} = \frac{1}{2}\frac{e^2}{4\pi\epsilon_0}\sum_{i\neq j}^{N}\frac{\mathbf{r}_i\cdot\mathbf{r}_j - 3z_iz_j}{|Z_i^{(0)} - Z_j^{(0)}|^3}. \tag{32}$$

The discussion of the individual terms contained in Hamiltonian (28) proceeds in analogy to the one presented for the single-ion case. The electronic dynamics of each ion is governed by $H_{{\rm el},i}$ in (28) and is therefore dependent on the equilibrium positions of the ions. This gives rise to position-dependent electronic energies, i.e. $E_{nljm} \to E_{nljm,i}$ according to (12)–(14) with the ion-dependent gradients of (31).

We remark that even ions located at the edges of the ion chain experience qualitatively the same electric field configuration as an ion in the center of the trap. This is due to the fact that the electric field of the Paul trap is compensated by the field created by the ions themselves. Therefore, the ions do not exhibit permanent dipole moments and each ion can be considered to be located in the center of a local electric quadrupole field. This is the reason why the electronic properties of the system of trapped ions are virtually unaffected by the actual number of particles at hand.

The term of interest to create strong interactions among the ions is the dipole–dipole interaction. In the parameter regime where the interparticle distance ζ is much larger than the extension of the electronic wave function $a_{\rm Ry}$ of a Rydberg ion, the dipole-dipole interaction can be treated perturbatively. For the considered s and p states the expected interaction energy can be estimated by $E_{\rm vdW} \sim e^4|\langle n,\mathrm{s}|r|n,\mathrm{p}\rangle|^4/((4\pi\epsilon_0)^2|\triangle E_{\rm s,p}|\zeta^6)$. For Ca^+, $n = 50$ and $\zeta = 5\,\mu$m one finds $E_{\rm vdW} \sim \hbar \times 200\,$kHz. In the next subsection, we demonstrate that the MW fields introduced in section 2.3 in order to manipulate the electronic level structure can give rise to much stronger interactions among the ions.

3.2. Interaction between MW-dressed Rydberg ions

To study the interaction between MW-dressed Rydberg ions, we first transform the N-ion Hamiltonian (28) to a frame of reference, which rotates at the MW frequencies ω_1 and ω_2 of

the dressing fields (in analogy to the single-ion transformation in section 2.3). In the rotating frame, the terms in $H_{\mathrm{int-ext}}$ oscillate rapidly at the frequencies ω_1 and ω_2 and $\omega_1 - \omega_2$. Hence, in the rotating-wave approximation, the internal and external dynamics decouple (cf discussion in section 2.1).

We use the dressed ion Hamiltonian (18) and the expression (19) for the electronic dipole moment in order to represent the Hamiltonian $H_{\mathrm{int}} = \sum_i^N H_{\mathrm{el},i} + H_{\mathrm{dd}}$, which is part of the full Hamiltonian (28). The terms $H_{\mathrm{el},i}$ are replaced by the 2D representation given by (18). In this representation we can write the dipole–dipole interaction as

$$H_{\mathrm{dd}} = -\frac{1}{4\pi\epsilon_0}\sum_{i\neq j}^{N}\frac{d_z^{(i)}d_z^{(j)}}{|Z_i^{(0)} - Z_j^{(0)}|^3}, \tag{33}$$

where $d_z^{(i)}$ is given by (19) with the index i labeling the respective ions. In the rotating wave approximation, we obtain

$$\begin{aligned} H_{\mathrm{int}} = &\sum_i^N \mathbf{h}^{(i)}\mathbf{S}^{(i)} + D_1\sum_{i,j(\neq i)}^{N} v_{ij}\left[\frac{1}{4}\eta_i^2 + \eta_i\eta_j S_z^{(i)}\right] \\ &+ \sum_{i,j(\neq i)}^{N} v_{ij}\left[D_2\left(S_x^{(i)}S_x^{(j)} + S_y^{(i)}S_y^{(j)}\right) + \eta_i\eta_j D_1 S_z^{(i)}S_z^{(j)}\right], \end{aligned} \tag{34}$$

with $v_{ij} = -2/(4\pi\epsilon_0|Z_i^{(0)} - Z_j^{(0)}|^3)$ and an effective magnetic field $\mathbf{h}^{(i)} = \hbar(\Omega_2, 0, \Delta_2^{(i)})$. The coefficients $D_{1,2}$ and η_i characterize the coupling strengths and depend on the transition matrix elements between the involved Rydberg states and the MW dressing. As depicted in figure 3 the effective spin corresponds to a two-level system constituted by two MW-dressed Rydberg states (see section 2.3 for details).

The terms linear in the spin operators represent a coupling of a series of spins to an inhomogeneous effective magnetic field whose strength and direction are determined by the position-dependent electronic energies of the Hamiltonian (30). The terms in the second line of (34) (quadratic in the spin operators) represent a ferromagnetic Heisenberg chain with $1/r^3$ exchange-type interaction [24]. Establishing the connection to neutral Rydberg gases the $S_x^{(i)}S_x^{(j)}$ and $S_y^{(i)}S_y^{(j)}$ can be interpreted as resonant dipole–dipole interaction terms. The term that is proportional to $S_z^{(i)}S_z^{(j)}$ resembles the interaction of two static dipoles. In general, the coefficients $\eta_i = \Omega_1^{(i)}/(2\Delta_1^{(i)})$ depend on the ion index, since different energy shifts of the $|n', \mathrm{p}\rangle$ level due to position-dependent charge-quadrupole terms (cf (30) and (31)) lead to different detunings $\Delta_1^{(i)}$ for different ions (see figure 5). In case one does not admix the $|n', \mathrm{p}\rangle$ state to $|n, \mathrm{s}\rangle$ (i.e. $\Omega_1 = 0$ in (16)), the coefficients η_i vanish and the interaction Hamiltonian solely describes resonant dipole–dipole interaction in the presence of an effective magnetic field with a constant component in x and a position-dependent component in the z-direction.

In section 2.4, we have shown that the trapping frequencies for ions excited to Rydberg states can slightly differ from the ones of their ground-state counterparts. In appendix A, we show that this residual coupling leads to entanglement of the effective spin dynamics with the external motion of the ions. This results predominantly in dephasing in the effective spin dynamics, which limits the timescale of validity of Hamiltonian (34). We find that for typical parameters the dephasing time is of the same order or larger than the radiative lifetime of the Rydberg states. Thus, the limiting factor for the quality of a quantum simulation of the effective

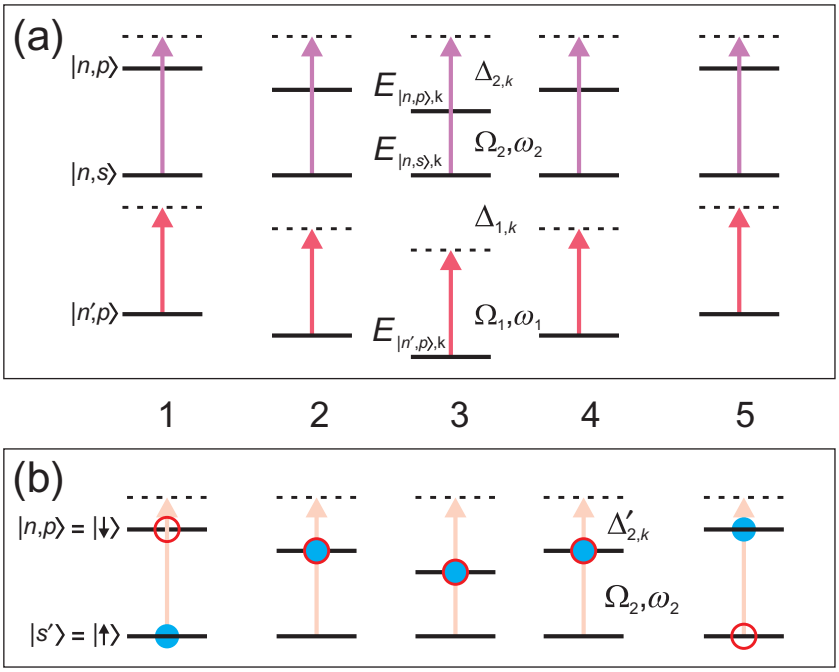

Figure 5. (a) Schematic level scheme of the three MW-coupled Rydberg levels, for a chain of five ions. The individual, position-dependent energy shifts of the $l = 1$ states give rise to an inhomogeneous distribution of MW detunings (not true to scale). (b) Schematic spin dynamics of a chain with the initial configuration: first ion in the $|n, \mathrm{p}\rangle$ state, all other ions in the $|\mathrm{s}'\rangle$ state (blue filled circles). After a certain time, the Rydberg excitation has traveled to the right end of the chain (red open circles). A numerical example of this excitation transfer is shown in figure 6.

spin dynamics of (34) and the fidelity of the two-qubit gate proposed in section 3.5 is set by the radiative decay of the involved Rydberg states (see also discussion below).

The dipole–dipole interaction can, in principle, lead to transitions to Rydberg pair-states which lie outside the manifold spanned by direct products of the states $|n, \mathrm{s}\rangle$, $|n, \mathrm{p}\rangle$. In this case one would have to include more than the two above-mentioned single-ion Rydberg states in order to describe the electronic degrees of freedom of an ion. However, one can always find a scenario (by choosing an appropriate principal quantum number) in which these pair states are sufficiently far detuned, i.e. much larger than the dipole–dipole coupling. In this case, unwanted transitions are strongly suppressed over the timescale of interest and the effective spin-$\frac{1}{2}$ description applies.

The physical realization of effective spin dynamics, as provided by the Hamiltonian (34), has been of significant interest in atomic physics during the last few years as 'analog quantum simulators' of (mesoscopic) condensed matter systems. The distinguishing feature of the present setup is the large coupling strength between effective spins, which scales proportional to n^4 and is of the order of $\hbar \times 500\,\mathrm{MHz}$ ($n \approx 50$, typical interparticle spacing $\zeta \approx 5\,\mu\mathrm{m}$). The characteristic timescale of the effective spin dynamics is thus of the order of a few nanoseconds. This is significantly shorter than the typical decoherence time in the system, which is set by the

radiative lifetimes of the involved Rydberg states, which scale as n^3 and are typically of the order of μs (for Ca^+ ions, $n = 50$ and the lifetime is $\sim 10\,\mu$s [20]).

Realization of effective spin models has also been proposed in the context of trapped ions in their electronic ground state, and with cold atoms and polar molecules in optical lattices. For trapped ions involving electronic ground states, models analogous to (34) can be derived where the typical coupling strengths for the effective spin–spin interactions are in the range of tens of kHz [16] with (long) decoherence times as described in the context of ion trap quantum computing [25, 26]. Effective Heisenberg models with nearest-neighbor interactions are also obtained with cold atoms in optical lattices [27, 28], where the timescales of exchange interactions can be of the order of a few hundred Hz [29, 30]. We note that these energy scales are also directly related to the temperature requirements for the preparation of an effective zero-temperature ensemble. Finally, effective spin models, such as the Kitaev model [31], have been proposed with polar molecules in optical lattices [32]–[34]. In this context, electric dipole moments of a few Debyes can be induced by external dc and MW electric fields in the rotational manifold of molecules prepared in their electronic and vibrational ground state. The electric dipole–dipole interactions, which are strong and long-range in comparison with neutral atom collisional interactions, can lead to effective offsite-coupling strengths of the order of tens or hundreds of kHz, limited mainly by the conditions imposed by optical trapping, while coherence times are of the order of seconds, as determined e.g. by spontaneous emission in off-resonant light fields forming the trapping potential.

A second feature of simulating spin dynamics according to Hamiltonians of the type (34) is the single-ion addressability and read out [35], which the present setup inherits from the experimental developments in ion-trap quantum computing. In contrast, neutral atoms and molecules in optical molecules usually allow global addressing by laser light, even though significant effort is being devoted at the moment to developing these tools also for optical lattice setups [36, 37]. Note, however, that neutral atoms and molecules in optical lattices will typically allow for systems with a significantly larger number of 'spins' than in the ion case. In contrast, ion chains with their smaller number of constituents allow for implementing and studying mesoscopic versions of quantum many-body models [38].

One of the experimentally most challenging aspects of realizing a Rydberg ion chain is the requirement of π-pulses to transfer ions from the ground state to the Rydberg state. In section 3.4, we discuss a version of an effective spin chain where the Rydberg dipoles are admixed to the electronic ground states with an off-resonant laser process, resulting in ground-state ions with effective oscillating dipole moments.

3.3. Resonant excitation transfer

In recent years, great attention has been devoted to quantum spin chains as described by the Hamiltonian (34) as candidate systems for the implementation of quantum channels for short-distance quantum communication [39]. Here, a certain quantum state is placed on one spin of the chain and dynamically transferred to a distant spin of the chain within a certain time and with some fidelity (for an overview of quantum communication via spin chains, see e.g. [40] and references therein). It has also been suggested to use (disordered) spin chains for the purpose of quantum computation [41, 42]. A large variety of physical systems (see e.g. [43] for further references) has been proposed as realizations of quantum spin chains, reaching from Josephson

junctions with charge and flux qubits over quantum dots, NMR qubits, optical lattices to coupled arrays of cavities.

In view of practical implementations of such quantum channels, it has been studied in particular how the fidelity of the quantum-state transfer is affected by static and time-dependent inhomogeneities and disorder both in the spin couplings and the local magnetic fields applied to the individual spins [44]–[49], and how even single defects may drastically alter the transport properties through the chain [50].

As an illustration of the spin dynamics contained in Hamiltonian (34), which exhibits inhomogeneities both in the exchange couplings and the effective magnetic field, we study the transfer of an excitation from one side of a chain of ten ions to the other end. For simplicity we choose a scenario in which $\eta_i = 0$ ($\Omega_1 = 0$ in (16)). As discussed in the previous subsection, in this case the interaction reduces to purely resonant dipole–dipole interaction. The ion-dependent coefficient of the dipole–dipole interaction can be written as

$$\nu_{ij} = -\frac{2}{4\pi\epsilon_0 |Z_i^{(0)} - Z_j^{(0)}|^3} = -\frac{2M\omega_z^2}{e^2}\frac{1}{|u_i - u_j|^3}, \tag{35}$$

where the u_i are the equilibrium positions in dimensionless coordinates, $u_i = Z_i^{(0)}/\zeta$ with $\zeta = [e^2/(4\pi\epsilon_0 M\omega_z^2)]^{1/3}$ (see [15]). The scale of the interaction energy is then given by $J = -(2M\omega_z^2/e^2)D_2$. We choose the MW frequency ω_2 such that it is in resonance with the energy gap between the levels $|n, \mathrm{s}\rangle$ and $|n, \mathrm{p}\rangle$ determined by the gradient (31) with $\delta\beta_i = 0$. Following (14), the position-dependent change of the gradient $\delta\beta_i$ gives rise to a position-dependent variation of the detuning, which reads

$$\begin{aligned}\triangle_{2,i} &= -\frac{4}{5} e\,\delta\beta_i \langle n, \mathrm{p}|r^2|n, \mathrm{p}\rangle \\ &= -\frac{2}{5} M\omega_z^2 \langle n, \mathrm{p}|r^2|n, \mathrm{p}\rangle \sum_{j\neq i}^{N} \frac{1}{|u_i - u_j|^3} = B_z \sum_{j\neq i}^{N} \frac{1}{|u_i - u_j|^3}.\end{aligned} \tag{36}$$

This situation is depicted in figure 5. The effective magnetic field B_z and the coupling constant J do not scale independently since both D_2/e^2 and the matrix element $\langle n, \mathrm{p}|r^2|n, \mathrm{p}\rangle$ are of the order of $a_0^2 n^4$. The precise value depends on the ionic species. For our simulations we use the parameters $B_z = 0.65\,J$ and $\hbar\Omega_2 = 0.01\,J$. Initially, the system is prepared by a series of π-laser pulses in such a way that the first ion ($k = 1$) is in the state $|\uparrow\rangle = |n, \mathrm{s}\rangle$, while all others are in the state $|\downarrow\rangle = |n, \mathrm{p}\rangle$. This state is sketched in figure 5(b) by the solid circles. The temporal evolution under the Hamiltonian (34) leads to a transfer of the excitation from the first ion to the last ion in the chain (open circles in figure 5(b)). The corresponding numerical data are shown in figure 6 where we monitor the time evolution of the expectation value $\langle S_z^{(i)}\rangle$ in a chain of ten ions. The excitation transfer from the first to the tenth ion takes place in a time $t = 1.8\hbar/J$ with an efficiency of 89%. Since J can be in the order of $\hbar \times 500$ MHz this resonant excitation transfer can therefore be achieved in about 3.6 ns, which is much less than the lifetime of ionic Rydberg states. The final state of the effective spin chain could be measured by first transferring the ions from the $|n, \mathrm{s}\rangle$ and $|n, \mathrm{p}\rangle$ states to two internal (meta-)stable states, and by subsequently applying standard fluorescence-state tomography techniques [35].

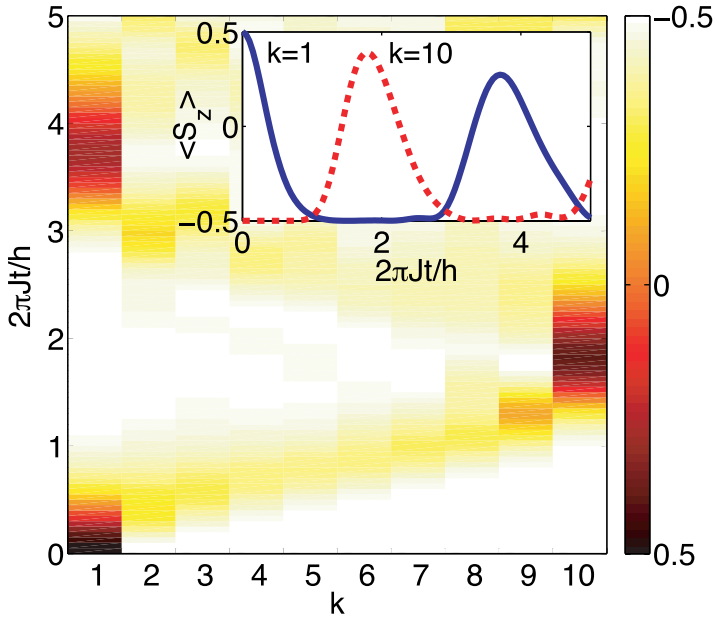

Figure 6. Transport of an excitation through a chain of ten ions. The ion at site 1 is initially excited to the state $|\uparrow\rangle$, while all others are in the state $|\downarrow\rangle$. After the time $t = 1.8\,\hbar/J$, the excitation is transferred from the first to the tenth ion. The inset shows the time evolution of the expectation values $\langle S_z^{(1)}\rangle$ and $\langle S_z^{(10)}\rangle$.

3.4. Spin dynamics in the electronic ground states

In view of the short transition wavelength of 100 . . . 125 nm associated with a transition from an electronic ground state to a Rydberg level[5], it is experimentally challenging to realize π laser pulses, which transfer the entire electronic population to the Rydberg levels, as required for the initialization step of the chain of effective spins. Thus, we outline an alternative scheme, which does not require the transfer of the full electronic population to Rydberg states and which is based on an adiabatic admixture of Rydberg levels to two electronic ground states by near-resonant CW lasers.

We extend the three-level scheme of section 2.3 by including two ground states $|g_1\rangle$ and $|g_2\rangle$, which are coupled by two lasers to the (undressed) Rydberg states $|n, \mathrm{s}\rangle$ and $|n, \mathrm{p}\rangle$, respectively (see figure 7). As before, we use the MW dressing fields to couple the set of bare Rydberg states $|n', \mathrm{p}\rangle$, $|n, \mathrm{s}\rangle$ and $|n, \mathrm{p}\rangle$. The two CW lasers weakly couple the two ground states to the resulting dressed Rydberg level structure. Weak coupling requires that the laser Rabi frequencies are small compared with the MW Rabi frequencies and that the laser fields are sufficiently far detuned from the three dressed Rydberg states. Owing to the laser coupling, the two dressed ground states $|g_1'\rangle$, $|g_2'\rangle$ obtain time-dependent oscillating dipole moments, which finally lead to dipole–dipole interactions between laser-dressed *ground-state* ions. The dressed ground states now constitute the two-level system of interest (effective spin degree of freedom) and play the role of the dressed Rydberg levels $|\mathrm{s}'\rangle$ and $|n, \mathrm{p}\rangle$ of section 2.3.

As shown in appendix D for a specific set of Rabi frequencies and detunings of the MW and laser fields, the representation of the dipole operator in this effective two-level

[5] Spectral data for different ion species can be found, e.g. in [51].

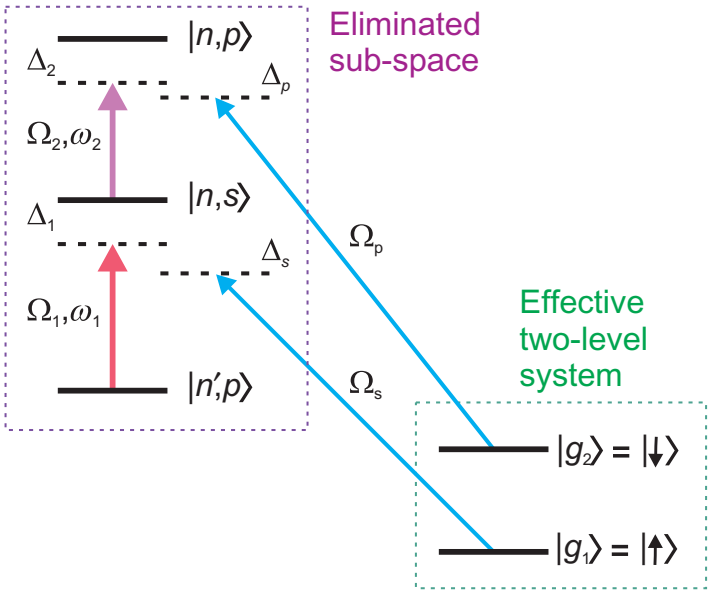

Figure 7. MW dressing of ground state ions. Two lasers with Rabi frequencies Ω_s, Ω_p and detunings Δ_s, Δ_p weakly couple two electronic ground states $|g_1\rangle$, $|g_2\rangle$ to the Rydberg levels $|n, s\rangle$ and $|n, p\rangle$, respectively. Thus ions residing in the electronic ground states are dressed and obtain time-dependent oscillating dipole moments.

system reads

$$d_z = \begin{pmatrix} 0 & c_{p,1}c_{s,2}\sqrt{D_2}\,e^{-i\omega_2 t} \\ c_{p,1}c_{s,2}\sqrt{D_2}e^{i\omega_2 t} & 2c_{s,2}c_{p',2}\sqrt{D_1}\cos(\omega_1 t) \end{pmatrix}$$

$$= c_{s,2}c_{p',2}\sqrt{D_1}\cos(\omega_1 t)(1-2S_z) + 2c_{p,1}c_{s,2}\sqrt{D_2}(\cos(\omega_2 t)S_x + \sin(\omega_2 t)S_y) \tag{37}$$

with the factors c_α given by (D.7). Thus, the resulting dipole operator as well as the resulting spin chain Hamiltonian describing the dynamics in the dressed ground states $|g_1'\rangle$, $|g_2'\rangle$ have the same structure as in (20) and (34), with the difference that the magnitude of the dipole moments is decreased by the factors $c_{p,1}c_{s,2}$ and $c_{p',2}c_{s,2}$, respectively.

Owing to the weak admixture of the Rydberg states, the dressed ground states, have a finite lifetime, i.e. the time until a photon of the dressing lasers is scattered. Denoting the lifetime of the involved Rydberg states by $\tau = 1/\Gamma$, this scattering rate is approximately given by $\Gamma_{scat} = |c_\alpha|^2\Gamma$, where c_α represents a typical value of the admixture coefficients in (D.7). For instance, the lifetime of the state $|g_1'\rangle$ is enhanced by a factor of $|c_{p,1}|^{-2}$ with respect to the radiative lifetime of the Rydberg state $|n, p\rangle$, since only the fraction $|c_{p,1}|^2$ of the electronic population resides in the Rydberg state. Moreover, the fraction of the admixed Rydberg states affects the interaction among the ions. Compared with the bare dipole–dipole interaction the interaction between the dressed ions is suppressed by a factor $\sim |c_\alpha|^4$, resulting in an effectively slower spin dynamics. The typical timescale for the spin dynamics, e.g. the excitation transfer discussed in section 3.2, thus increases proportional to $|c_\alpha|^{-4}$. Hence, comparison of the scaling of the interaction strength and the lifetime reveals that the adiabatic admixture of Rydberg

states must not be too weak in order to avoid that the decoherence due to spontaneous emission becomes an issue during the temporal evolution of the spin dynamics.

We remark that the outlined scheme for dressed ground-state ions also possesses the advantage that—in contrast with the situation where the ions are excited to Rydberg states—it does not require a transfer of the electronic population from the Rydberg to (meta-)stable states before performing the quantum-state tomography.

3.5. Fast two-qubit quantum gates with Rydberg ions

In most two-qubit gate schemes, which have been suggested and implemented so far with trapped ions (see [52]–[54] for a few examples), the motional sidebands of the ions have to be spectroscopically resolved, which limits the achievable gate operation times, typically to the order of the inverse external trapping frequency. In order to overcome this limitation, it has been proposed to use specifically shaped trains of off-resonant laser pulses to implement geometric two-qubit ion gates with much faster gate times [55]. In the context of quantum information processing with neutral atoms, potentially fast two-qubit gates can be achieved for pairs of Rydberg atoms in an optical lattice, based on the strong and long-range dipolar interactions among the atoms [2, 8, 56].

For the system of trapped Rydberg ions we have shown that despite the absence of permanent dipole moments MW-dressing fields can be used to generate strong dipole–dipole interactions between Rydberg ions. We now aim to exploit the electronic interaction Hamiltonian (34) for the implementation of a fast conditional two-qubit phase gate along the lines of the proposals developed for neutral Rydberg atoms. Such a gate is characterized by the truth table $|g_a\rangle_m|g_b\rangle_n \to \mathrm{e}^{\mathrm{i}(a-2)(b-2)\phi_{\mathrm{ent}}}|g_a\rangle_m|g_b\rangle_n$ with $a, b = 1, 2$ labeling the two ground states, and the ion indices m, n. Thus, the two-qubit state $|g_1\rangle_m|g_1\rangle_n$ obtains a phase shift, while the other three states are unaffected (up to trivial single-qubit phases) [57].

We identify the two ground states $|g_1\rangle_m$ and $|g_2\rangle_m$ of each ion m as logical qubit states $|0\rangle$ and $|1\rangle$. The ground state $|g_1\rangle$ is coupled to the Rydberg state $|n, \mathrm{s}\rangle$ by a near-resonant laser with time-dependent effective Rabi frequency $\Omega_{\mathrm{s}}(t)$ and detuning $\Delta_{\mathrm{s}}(t) = \omega_{\mathrm{s}}(t) - (E_{|n,\mathrm{s}\rangle} - E_{|g_1\rangle})/\hbar$, which can be chosen equal for both ions m and n. The second ground state $|g_2\rangle$ is not coupled to any Rydberg state. We again consider the scenario in which only one additional MW field with Rabi frequency Ω_2 and ion-dependent detunings $\Delta_{2,m}$ (cf section 3.2) is applied (see figure 8), i.e. $\Omega_1 = 0$ and $\eta_m = 0$ in (34). To perform the gate operation, we apply laser pulses to the two ions (similarly to the adiabatic gate scheme presented in [8]). The variation of the laser pulses is assumed to be slow on the timescale set by Ω_{s} and Δ_{s} such that the system follows adiabatically the dressed states, which arise from slowly switching on the laser coupling. This adiabaticity condition guarantees that after applying the laser pulses the electronic population still completely resides in the initial electronic ground states. During the application of the laser pulses and the resulting dressing of the electronic ground states, part of the electronic population is transferred from the states $|g_1\rangle_m$ and $|g_1\rangle_n$ to the Rydberg states, where the ions interact via the resonant dipole–dipole interaction and thereby accumulate an entanglement phase, given by

$$\phi_{\mathrm{ent}}(t) = \int_0^t \mathrm{d}\tau\,(\epsilon_{|g_1\rangle|g_1\rangle}(\tau) - \epsilon_{|g_1\rangle|g_2\rangle}(\tau) - \epsilon_{|g_2\rangle|g_1\rangle}(\tau)), \tag{38}$$

where $\epsilon_{|g_a\rangle_m|g_b\rangle_n}$ denotes the eigenenergy of the instantaneous eigenstate connected to the state $|g_a\rangle_m|g_b\rangle_n$ in the absence of laser pulses. Figure 9(a) shows a specific choice for the pulse

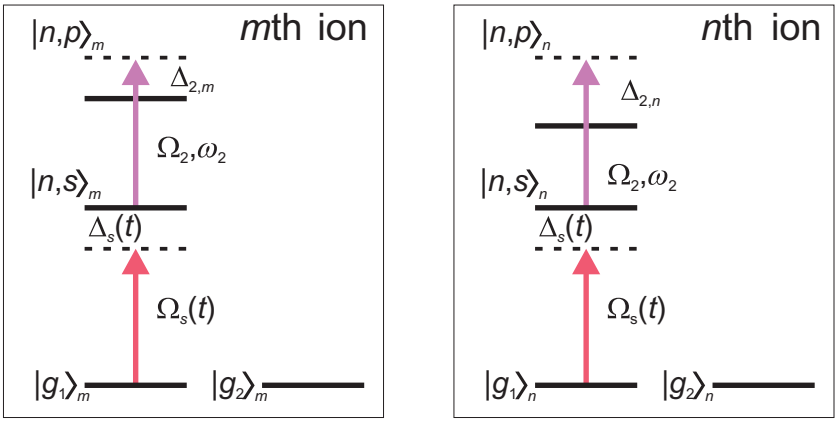

Figure 8. Level scheme for the implementation of a conditional two-qubit phase gate. The ground states $|g_1\rangle$ of the respective ions are coupled via a laser with time-dependent detuning $\Delta_s(t)$ and Rabi frequency $\Omega_s(t)$ to the Rydberg level $|n, s\rangle$. A MW field of constant Rabi frequency Ω_2 and ion-dependent detuning $\Delta_{2,m}$ couples the Rydberg levels $|n, s\rangle$ and $|n, p\rangle$.

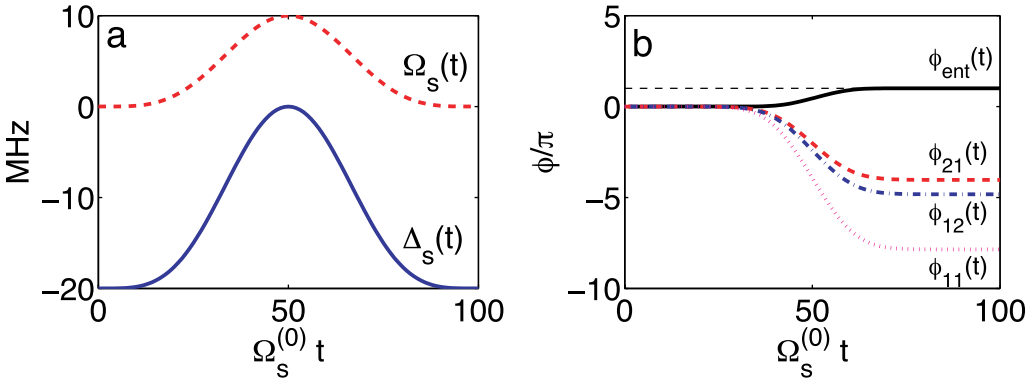

Figure 9. Two-qubit conditional phase gate between the first and second ion in a chain of ten ions. (a) Pulse profile: Rabi frequency $\Omega_s(t)$ and detuning $\Delta_s(t)$ of the dressing lasers. The MW Rabi frequency is chosen $\Omega_2 = 57.5$ MHz, the ion-dependent MW detunings are $\Delta_{2,1} = -279$ MHz, $\Delta_{2,2} = -667$ MHz. Dipole–dipole interaction energy scale $J/\hbar = 500$ MHz (cf section 3.2). (b) Accumulated phase shifts in the dressed states adiabatically connected to the initial ground states, and resulting entanglement phase $\phi_{\text{ent}}(t)$.

profile, the time-dependent energies of the dressed states adiabatically connected to the different ground states. The resulting accumulated phase shifts are presented in figure 9(b). The gate operation time T is approximately two orders of magnitude larger than the inverse of the maximum Rabi frequency $\Omega_s^{(0)}$ of the applied lasers in order to satisfy the adiabaticity condition (for the chosen set of parameters, $T = 100/\Omega_s^{(0)} = 10\,\mu$s). In order to minimize imperfections in the gate operation due to spontaneous scattering of photons of the dressing lasers (cf the discussion in section 3.4), the gate operation has to take place on a timescale much faster than

the lifetime τ of the involved Rydberg levels, i.e. $T \ll \tau$. Furthermore, T has to be shorter than the dephasing time t_{deph}, which results from the residual coupling of the electronic dynamics and the external motion (cf the discussion in section 3.2 and appendix A). For sufficiently high laser Rabi frequencies and long-lived Rydberg levels, these conditions can be satisfied.

4. Conclusions and outlook

In this paper, we have shown that trapping of Rydberg ions in a linear electric ion trap under realistic conditions is feasible. We have found that for not too large principal quantum numbers, electronic losses and field ionization of the Rydberg ions due to the trapping fields are negligible, and that the coupling of electronic and external dynamics of the ions results in renormalized trapping frequencies for ions excited to Rydberg states. We have suggested to use MW dressing fields in order to generate strong dipolar interactions among the ions. The Rydberg excitation dynamics of the MW-dressed ions can be described by an effective interacting spin-$\frac{1}{2}$ Hamiltonian. The strong interactions give rise to a typical corresponding timescale of the order of a few ns, which is substantially shorter than the typical decoherence time set by the radiative decay of Rydberg states. We have studied the dynamical transfer of a Rydberg excitation through the ion chain and discussed the implementation of fast two-qubit gates. While the laser excitation of ions to Rydberg states is an experimentally challenging task, the system offers the prospect of studying coherent many-body quantum dynamics on fast timescales in a well-controlled and structured environment.

Beyond the present work, trapped Rydberg ions offer a rich playground for further studies of more involved Rydberg dynamics: Combining e.g. ions of different species or exciting only a certain number of the trapped ions to Rydberg states offers the possibility of introducing further inhomogeneities in the spatial distribution of effective spins and of studying in a well-controlled way spin chain dynamics in the presence of disorder and effective spin vacancies (cf the discussion in section 3.3). The analysis can also be readily extended to the study of Rydberg excitation dynamics in 2D or 3D ion crystals. The individual addressability of trapped Rydberg ions allows for the setup of an excitation trap [9], where an effective spin excitation propagating along the ion chain is trapped or extracted from the system once it reaches a dedicated site.

The present work focuses on the parameter regime where the interparticle distance in the ion chain is much larger than the extension of the electronic wave function of ions excited to Rydberg states. Another interesting scenario is the situation where those two length scales become comparable. If this regime can be achieved, electrons could hop between overlapping Rydberg orbitals of adjacent ions, which would pave the way towards the realization of mesoscopic Hubbard-type models in an ion trap.

Acknowledgments

We thank Klemens Hammerer, Andreas Buchleitner, Hartmut Häffner, Piet Schmidt and Rainer Blatt for discussions, and in particular Jonathan Home for valuable comments. This work was supported by the Austrian Science Foundation, the EU under grants CONQUEST, MRTN-CT-2003-505089 and SCALA IST-15714, and the Institute for Quantum Information. L-ML acknowledges funding from the National Funds of Natural Science (grant no 10504042).

Appendix A. Residual entanglement of internal and external motion

In this appendix, we discuss the influence of the renormalized trapping frequencies (24) and (25) on the quality of the effective spin model (34) and the quantum gate proposed in section 3.5.

The basic effect of the coupling of internal and external dynamics can be understood by considering a simple model system. It consists of a driven two-level system (corresponding to the $|n, \mathrm{s}\rangle$ and $|n, \mathrm{p}\rangle$ Rydberg states), which is coupled to a harmonic oscillator mode (describing the external confinement of the ion) through a state-dependent frequency shift $\delta\omega$ of the oscillator (we assume $|\delta\omega| \ll \omega$):

$$H = \frac{p^2}{2m} + \frac{m\omega^2}{2}x^2 + \frac{\hbar\Delta}{2}\sigma_z + \frac{\hbar\Omega}{2}\sigma_x + \frac{\hbar(\delta\omega)}{x_{\mathrm{ho}}^2}x^2 \otimes \sigma_z. \tag{A.1}$$

Here, $x_{\mathrm{ho}} = \sqrt{\hbar/(m\omega)}$ is the oscillator length and $\sigma_{x,z}$ are Pauli matrices. On introducing creation and annihilation operators, the Hamiltonian takes the form

$$H = \hbar\omega a^\dagger a + \frac{\hbar\Delta'}{2}\sigma_z + \frac{\hbar\Omega}{2}\sigma_x + \hbar(\delta\omega)a^\dagger a \otimes \sigma_z + \frac{\hbar(\delta\omega)}{2}\left(a^{\dagger 2} + a^2\right) \otimes \sigma_z \tag{A.2}$$

with the renormalized detuning $\Delta' = \Delta + (\delta\omega)$. After transforming to an interaction frame with respect to the free evolution of the oscillator, the Hamiltonian reads

$$H' = \frac{\hbar\Delta'}{2}\sigma_z + \frac{\hbar\Omega}{2}\sigma_x + \hbar(\delta\omega)a^\dagger a \otimes \sigma_z + \frac{\hbar(\delta\omega)}{2}\left(\mathrm{e}^{-2\mathrm{i}\omega t}a^{\dagger 2} + \mathrm{e}^{2\mathrm{i}\omega t}a^2\right) \otimes \sigma_z. \tag{A.3}$$

The rotating terms describe off-resonant couplings between different oscillator levels, which yield corrections of the order of $(\delta\omega)^2/\omega$ and can be neglected. The dominant perturbation comes from the term $\hbar(\delta\omega)a^\dagger a \otimes \sigma_z$, which is diagonal in the basis of oscillator number states and results in dephasing of the two-level dynamics. The characteristic dephasing time can be estimated as $\tau_{\mathrm{deph}} \sim [(\delta\omega)\langle\Delta n\rangle]^{-1}$, where $\langle\Delta n\rangle$ denotes the variance in the initial occupation number distribution of the oscillator mode.

The real physical system under consideration consists of N effective spins encoded in the two Rydberg states of each ion, while the external motion of the ion string is described by $3N$ oscillator (phonon) modes. In section 2.4, we have found that the renormalization of the radial trapping frequency is approximately two orders of magnitude larger than for the longitudinal one. This implies that the dephasing of each individual spin-$\frac{1}{2}$ system mainly results from the coupling to the two vibrational modes in the X- and Y-directions. The dephasing time for a quantum state of N spins obviously strongly depends on the actual spin state under consideration. A rough estimate yields an expected reduction of at most by a factor of $1/(2N)$ compared with a single spin coupled to a single oscillator mode: $\tau_{\mathrm{deph},N} \approx \tau_{\mathrm{deph}}/(2N)$. For a chain of ten ions with sideband-cooled radial modes (see e.g. [58]) and a relative correction of the radial trapping frequency of 0.1%, we find dephasing times $\tau_{\mathrm{deph},N=10}$ of several μs, which is of the same order of magnitude as the radiative lifetime of the ions.

Appendix B. Electronic losses and ionization

In this appendix, we discuss under which conditions unwanted loss of electronic population from the Rydberg states $|n, \mathrm{s}\rangle$ and $|n, \mathrm{p}\rangle$ and ionization effects due to the static and time-dependent trapping fields and the MW dressing fields contained in Hamiltonian (12) are negligible.

We first analyze the effect of the static term $H_{\rm stat}$ and consider the potential

$$V' = -\frac{2e^2}{4\pi\epsilon_0 r} + e\beta\left[x^2 + y^2 - 2z^2\right]. \tag{B.1}$$

Here we have approximated the interaction of the ionic core with the valence electron by a pure Coulomb potential. V' possesses two saddle points located at the z-axis at $z_{\rm sad} = \pm[e/(8\pi\epsilon_0\beta)]^{1/3}$, where it assumes the value $V'_{\rm sad} = -\frac{3}{2}\left[(e^5\beta)/(\epsilon_0^2\pi^2)\right]^{1/3}$. Solving $E_{\rm Ry} = V'_{\rm sad}$ yields an estimate for the gradient β at which field ionization would occur classically,

$$\beta_{\rm ion} = \frac{4}{27}\frac{e^7 m^3}{(4\pi\epsilon_0)^4\hbar^6 n^6} = 1.44\times 10^{21}\,{\rm V\,m^{-2}} \times \frac{1}{n^6}. \tag{B.2}$$

For $n = 50$, for example, we find $\beta_{\rm ion} = 9.2\times 10^{10}\,{\rm V\,m^{-2}}$, which is three orders of magnitude larger than the largest values for the gradient β actually used in experiment [12].

In section 2.3, we use the MW dressing fields of (12) with Rabi frequencies Ω of the order of $2\pi\times$ 10 MHz for driving the $|n, {\rm s}\rangle \to |n, {\rm p}\rangle$ transition. The fields might cause unwanted electronic population transfer from these two states of interest to near-resonant Rydberg levels with subsequent ionization. For Ca^+ it can be seen from the level scheme (cf figure 2(a)) that no accidental quasi-degeneracy of the $|n, {\rm s}\rangle \to |n, {\rm p}\rangle$ transition with transitions to other Rydberg states exists. Thus, single-photon transitions leading out of the two-level system are far off-resonant[6]. Consequently, also multiphoton Raman-type transitions are strongly suppressed due to the large detuning to any possible intermediate state. 'True' n-photon transitions can be ruled out, since we work in the regime where $\Omega \ll \omega$ with ω being the MW frequency [1].

It is known that time-dependent electric fields can lead to ionization of Rydberg states at field strengths far below the threshold expected for a static field of the same strength [59]–[61]. The underlying mechanism is a series of Landau–Zener transitions between states belonging to different n-manifolds. In the case of a homogeneous electric field, they become significant around a field strength of $(eQ^3)/((4\pi\epsilon_0)3a_0^2n^5)$, which corresponds to the Inglis–Teller limit [1] (Q is the core charge). We apply a similar argument for the gradient field $H_{\rm osc}$ in (12). Estimating the maximal first-order energy shift of the uppermost state of the n-manifold as $e\alpha a_0^2 n^4/Q^2$ yields a critical field gradient of the order of

$$\alpha_c \approx \frac{1}{2}\frac{e}{(4\pi\epsilon_0)a_0^3} \times \frac{Q^4}{n^7}. \tag{B.3}$$

For $n = 50$ and singly charged ions, we find $\alpha_c \sim 10^{11}\,{\rm V\,m^{-2}}$, which is two orders of magnitude larger than typical experimental values [12].

Due to the strong modulation of the electric gradient field (cf discussion in section 2.2), multiphoton transitions out of the $|n, {\rm s}\rangle$, $|n, {\rm p}\rangle$ states, involving up to $\approx e\alpha a_0^2 n^4/(\hbar\omega_{\rm RF})$ photons, might occur. For Ca^+ and $n = 50$, the energy separation of about $2\pi\times 4$ GHz that could be bridged via such multiphoton transitions is still significantly smaller than the detuning of any transition leading out of the $|n, {\rm s}\rangle$, $|n, {\rm p}\rangle$ states.

In conclusion, for typical trap parameters and the MW field strengths we are interested in unwanted losses of electronic population for ions excited to the $|n, {\rm s}\rangle$, $|n, {\rm p}\rangle$ states and ionization due to the static and time-dependent trapping fields and the MW dressing fields is negligible for principal quantum numbers up to $n = 50$.

[6] For Ca^+ and $n = 50$, the transition frequency for the $|n, {\rm s}\rangle \to |n, {\rm p}\rangle$ transition of interest is $2\pi\times 84$ GHz, while the other relevant transitions are far off-resonant: $2\pi\times 153$ GHz for $|n, {\rm s}\rangle \to |n-1, {\rm p}\rangle$, $2\pi\times 43$ GHz for $|n, {\rm p}\rangle \to |n-1, {\rm d}\rangle$ and $2\pi\times 143$ GHz for $|n, {\rm p}\rangle \to |n+1, {\rm s}\rangle$ (no fine-structure included).

Appendix C. Hamiltonian of *N* interacting Rydberg ions

In this appendix, we derive the Hamiltonian for a system of N interacting trapped Rydberg ions. Using the single-ion Hamiltonian (6) and introducing a label for the respective ions, we find

$$H_N = \sum_i^N H_i' + \frac{1}{2}\sum_{i,j(\neq i)}^N V(\mathbf{R}_i, \mathbf{R}_j, \mathbf{r}_i, \mathbf{r}_j). \tag{C.1}$$

with V given by (26). The external dynamics is governed by the interplay of the harmonic confinement and the Coulomb force between the ions. The corresponding potential reads

$$V_{\text{ext}} = \frac{1}{2}M\sum_i^N \left[\omega_z^2 Z_i^2 + \omega_\rho^2 (X_i^2 + Y_i^2)\right] + \frac{1}{2}\frac{e^2}{4\pi\epsilon_0}\sum_{i,j(\neq i)}^N \frac{1}{R_{ij}}. \tag{C.2}$$

Following [16, 17], we perform a harmonic expansion of V_{ext}, which puts us in a position to describe the external dynamics in terms of uncoupled harmonic oscillators/phonon modes. To this end, we first calculate the ionic equilibrium positions $\mathbf{R}_i^{(0)}$. In a linear Paul trap with tight transversal confining, $\omega_\rho \gg \omega_z$, the ions align along the z-axis of the trap such that $\mathbf{R}_i^{(0)} = (0, 0, Z_i^{(0)})$ where the $Z_i^{(0)}$ are determined by $(\partial V_{\text{ext}}/\partial Z_i) = 0$, which leads to the system of equations

$$M\omega_z^2 Z_i^{(0)} = \frac{e^2}{4\pi\epsilon_0}\sum_{j(\neq i)}^N \frac{Z_i^{(0)} - Z_j^{(0)}}{|Z_i^{(0)} - Z_j^{(0)}|^3}. \tag{C.3}$$

With the $Z_i^{(0)}$ being determined, the harmonic approximation of the potential V_{ext} reads

$$V_{\text{ext}} = \frac{1}{2}M\sum_{\alpha=x,y,z}\sum_{i,j}^N K_{ij}^\alpha q_i^\alpha q_j^\alpha \tag{C.4}$$

with the displacements $q_i^x = X_i$, $q_i^y = Y_i$ and $q_i^z = Z_i - Z_i^{(0)}$ and the coefficient matrix

$$K_{ij}^\alpha = \begin{cases} \omega_\alpha^2 - c_\alpha \frac{e^2}{4\pi\epsilon_0 M}\sum_{k(\neq i)}^N \frac{1}{|Z_i^{(0)} - Z_k^{(0)}|^3}, & \text{for} \quad i = j, \\ c_\alpha \frac{e^2}{4\pi\epsilon_0 M}\frac{1}{|Z_i^{(0)} - Z_j^{(0)}|^3}, & \text{for} \quad i \neq j, \end{cases}$$

where $c_{x,y} = 1$, $c_z = -2$. The vibrational dynamics of the 1D chain is then described by

$$H_{\text{ph}} = \frac{1}{2}M\sum_{\alpha=x,y,z}\sum_{i,j}^N K_{ij}^\alpha q_i^\alpha q_j^\alpha + \frac{1}{2M}\sum_{\alpha=x,y,z}\sum_i^N (P_i^\alpha)^2. \tag{C.5}$$

The Hamiltonian H_{ph} can be brought into diagonal form by introducing phonon modes via the orthogonal matrices M^α,

$$q_i^\alpha = \sum_n^N \frac{M_{i,n}^\alpha}{\sqrt{2M\omega_{\alpha,n}/\hbar}}(a_{\alpha,n}^\dagger + a_{\alpha,n}), \tag{C.6}$$

$$P_k^\alpha = \mathrm{i}\sum_n^N \frac{M_{k,n}^\alpha}{\sqrt{2/(\hbar M\omega_{\alpha,n})}}(a_{\alpha,n}^\dagger - a_{\alpha,n}), \tag{C.7}$$

$$\sum_{i,j}^{N} M_{i,n}^{\alpha} K_{ij}^{\alpha} M_{j,m}^{\alpha} = \omega_{\alpha,n}^{2} \delta_{n,m}, \tag{C.8}$$

which leads to (29) for the phonon dynamics.

We now proceed by expanding the charge–dipole, the charge–quadrupole and the dipole–dipole interaction around the equilibrium positions of the ions. The charge–quadruple and the dipole–dipole interaction can be approximated by

$$H_{\mathrm{cq}} = \frac{1}{2}\frac{e^2}{4\pi\epsilon_0}\sum_{i\neq j}^{N}\frac{r_i^2 - 3(\mathbf{n}_{ij}\cdot\mathbf{r}_i)^2}{2R_{ij}^3} \simeq \frac{1}{2}\frac{e^2}{4\pi\epsilon_0}\sum_{i\neq j}^{N}\frac{r_i^2 - 3z_i^2}{2|Z_i^{(0)} - Z_j^{(0)}|^3}, \tag{C.9}$$

$$H_{\mathrm{dd}} = \frac{1}{2}\frac{e^2}{4\pi\epsilon_0}\sum_{i\neq j}^{N}\frac{\mathbf{r}_i\cdot\mathbf{r}_j - 3(\mathbf{n}_{ij}\cdot\mathbf{r}_i)(\mathbf{n}_{ij}\cdot\mathbf{r}_j)}{R_{ij}^3} \simeq \frac{1}{2}\frac{e^2}{4\pi\epsilon_0}\sum_{i\neq j}^{N}\frac{\mathbf{r}_i\cdot\mathbf{r}_j - 3z_i z_j}{|Z_i^{(0)} - Z_j^{(0)}|^3}. \tag{C.10}$$

The charge–quadrupole term leads to a position-dependent variation of the electric field and can be absorbed in the single-particle ion–field interaction H_{ef}, which is given by (12). The electronic Hamiltonian of the ith ion then assumes the form of (30) with the ion-dependent gradient (31).

In order to treat the charge–dipole coupling, we introduce the compact notation $r_i^x = x_i$, $R_i^x = X_i, \ldots$, which enables us to write

$$\begin{aligned} H_{\mathrm{cd}} &= \frac{1}{2}\frac{e^2}{4\pi\epsilon_0}\sum_{i\neq j}^{N}\frac{(\mathbf{R}_i - \mathbf{R}_j)(\mathbf{r}_i - \mathbf{r}_j)}{R_{ij}^3} \\ &\simeq \frac{1}{2}\frac{e^2}{4\pi\epsilon_0}\sum_{i\neq j}^{N}\frac{Z_i^{(0)} - Z_j^{(0)}}{|Z_i^{(0)} - Z_j^{(0)}|^3}(z_i - z_j) + \sum_{\alpha=x,y,z}\sum_{i,j(\neq i)}^{N}\frac{e^2}{4\pi\epsilon_0}\frac{1}{|Z_i^{(0)} - Z_j^{(0)}|^3}c_\alpha(r_i^\alpha - r_j^\alpha)q_i^\alpha. \end{aligned} \tag{C.11}$$

It turns out that by making use of the equilibrium condition (C.3), one can combine this expression with the term $\sum_i H_{\mathrm{CM-el},i}$ that arises from the summation of the single-ion terms of the Hamiltonian (6). The combination then includes all couplings between the internal and external dynamics. It reads

$$H_{\mathrm{int-ext}} = -2e\alpha\cos(\omega t)\sum_{i}^{N}[q_i^x x_i - q_i^y y_i] + \frac{1}{2}M\sum_{\alpha=x,y,z}\sum_{i,j}^{N}K_{ij}^z c_\alpha r_j^\alpha q_i^\alpha. \tag{C.12}$$

Finally, neglecting the micro-motion, the complete Hamiltonian of N Rydberg ions in the linear Paul trap is given by (29).

Appendix D. Effective dipole moment of laser-dressed ground state ions

In this appendix, we derive the form (37) of the dipole operator for laser-dressed ground state ions. The Hamiltonian for the system of five coupled electronic levels as depicted in figure 7 in the rotating frame is defined by the transformation

$$\begin{aligned} U(t) = {} & \mathrm{e}^{-\mathrm{i}\omega_s t}|g_1\rangle\langle g_1| + \mathrm{e}^{\mathrm{i}(\omega_2-\omega_p)t}|g_2\rangle\langle g_2| \\ & + \mathrm{e}^{-\mathrm{i}\omega_1 t}|n',\mathrm{p}\rangle\langle n',\mathrm{p}| + |n,\mathrm{s}\rangle\langle n,\mathrm{s}| + \mathrm{e}^{\mathrm{i}\omega_2 t}|n,\mathrm{p}\rangle\langle n,\mathrm{p}| \end{aligned} \tag{D.1}$$

and in rotating-wave-approximation is given by $H_{5\,\mathrm{levels}} = H_0 + H_{\mathrm{pert}}$,

$$H_0 = \hbar\Delta_\mathrm{s}|g_1\rangle\langle g_1| + \hbar\Delta_\mathrm{p}|g_2\rangle\langle g_2| + \hbar\Delta_1|n',\mathrm{p}\rangle\langle n',\mathrm{p}| - \hbar\Delta_2|n,\mathrm{p}\rangle\langle n,\mathrm{p}| + \frac{\hbar}{2}\left(\Omega_1|n',\mathrm{p}\rangle\langle n,\mathrm{s}| + \Omega_2|n,\mathrm{s}\rangle\langle n,\mathrm{p}| + \mathrm{h.c.}\right), \tag{D.2}$$

$$H_{\mathrm{pert}} = \frac{\hbar}{2}\left(\Omega_\mathrm{s}|g_1\rangle\langle n,\mathrm{s}| + \Omega_\mathrm{p}|g_2\rangle\langle n,\mathrm{p}| + \mathrm{h.c.}\right). \tag{D.3}$$

The MW detunings $\Delta_{1,2}$ and Rabi frequencies $\Omega_{1,2}$ are defined as in section 2.3, and the detunings and Rabi frequencies characterizing the two additional laser fields are given by $\Delta_\mathrm{s} = \omega_\mathrm{s} - (E_{|n,\mathrm{s}\rangle} - E_{|g_1\rangle})/\hbar$, $\Delta_\mathrm{p} = \omega_\mathrm{p} - (E_{|n,\mathrm{p}\rangle} - E_{|g_2\rangle})/\hbar - \Delta_2$ and Ω_s, Ω_p. We assume that the near-resonant MW fields are much stronger than the two lasers such that they determine the level structure of the dressed Rydberg states. Therefore we treat the coupling to the ground states as a perturbation H_{pert} of the system. We now apply a canonical transformation to the Hamiltonian [62],

$$e^{-S} H_{5\,\mathrm{levels}}\, e^{S} = H_0 + H_{\mathrm{pert}} + [H_0, S] + [H_{\mathrm{pert}}, S] + \cdots. \tag{D.4}$$

Choosing S such that $[H_0, S] = -H_{\mathrm{pert}}$, guarantees that to first order in the perturbation H_{pert}, the transformed Hamiltonian is block-diagonal and that the two ground states become decoupled from the Rydberg states. The transformation yields two dressed ground states, $|g'_{1,2}\rangle \simeq (1+S)|g_{1,2}\rangle$,

$$|g'_1\rangle = |g_1\rangle + c_{\mathrm{p}',1}|n',\mathrm{p}\rangle + c_{\mathrm{s},1}|n,\mathrm{s}\rangle + c_{\mathrm{p},1}|n,\mathrm{p}\rangle, \tag{D.5}$$

$$|g'_2\rangle = |g_2\rangle + c_{\mathrm{p}',2}|n',\mathrm{p}\rangle + c_{\mathrm{s},2}|n,\mathrm{s}\rangle + c_{\mathrm{p},2}|n,\mathrm{p}\rangle \tag{D.6}$$

with

$$\begin{pmatrix} c_{\mathrm{p}',1} \\ c_{\mathrm{s},1} \\ c_{\mathrm{p},1} \end{pmatrix} = \gamma_\mathrm{s} \begin{pmatrix} -(\Delta_\mathrm{s}+\Delta_2)\Omega_1 \\ 2(\Delta_1-\Delta_\mathrm{s})(\Delta_\mathrm{s}+\Delta_2) \\ (\Delta_1-\Delta_\mathrm{s})\Omega_2 \end{pmatrix}, \qquad \begin{pmatrix} c_{\mathrm{p}',2} \\ c_{\mathrm{s},2} \\ c_{\mathrm{p},2} \end{pmatrix} = \gamma_\mathrm{p} \begin{pmatrix} -\Omega_1\Omega_2 \\ 2(\Delta_1-\Delta_\mathrm{p})\Omega_2 \\ 4(\Delta_1-\Delta_\mathrm{p})\Delta_\mathrm{p} + \Omega_1^2 \end{pmatrix}, \tag{D.7}$$

where

$$\gamma_{\mathrm{s,p}} = \frac{\Omega_{\mathrm{s,p}}}{(\Delta_{\mathrm{s,p}}+\Delta_2)[4(\Delta_1-\Delta_{\mathrm{s,p}})\Delta_{\mathrm{s,p}} + \Omega_1^2] + (\Delta_{\mathrm{s,p}}-\Delta_1)\Omega_2^2}. \tag{D.8}$$

For the special choice of laser detunings

$$\Delta_\mathrm{s} = -\Delta_2, \qquad \Delta_\mathrm{p} = \tfrac{1}{2}\left(\Delta_1 - \sqrt{\Delta_1^2 + \Omega_1^2}\right), \tag{D.9}$$

we find

$$\begin{pmatrix} c_{\mathrm{p}',1} \\ c_{\mathrm{s},1} \\ c_{\mathrm{p},1} \end{pmatrix} = \begin{pmatrix} 0 \\ 0 \\ -\frac{\Omega_\mathrm{s}}{\Omega_2} \end{pmatrix}, \qquad \begin{pmatrix} c_{\mathrm{p}',2} \\ c_{\mathrm{s},2} \\ c_{\mathrm{p},2} \end{pmatrix} = \begin{pmatrix} \frac{\Omega_1\Omega_\mathrm{p}}{\Omega_2\left(\Delta_1+\sqrt{\Delta_1^2+\Omega_1^2}\right)} \\ -\frac{\Omega_\mathrm{p}}{\Omega_2} \\ 0 \end{pmatrix}. \tag{D.10}$$

Thus, for this set of parameters, the Rydberg state $|n, \mathrm{p}\rangle$ is exclusively admixed to the ground state $|g_1\rangle$, while the second ground state obtains a small fraction of the Rydberg states $|n', \mathrm{p}\rangle$ and $|n, s\rangle$. This implies that the dressed ground state $|g_2'\rangle$ possesses a non-vanishing dipole moment, which oscillates at the MW frequency ω_1, and that there exists also a transition dipole matrix element between the two dressed ground states. We now identify the two dressed ground states $|g_1'\rangle$, $|g_2'\rangle$ with the eigenstates of the S_z spin operator along the lines of section 2.3 and obtain the dipole operator (37).

References

[1] Gallagher T F 1984 *Rydberg Atoms* (Cambridge: Cambridge University Press)
[2] Lukin M D, Fleischhauer M, Côté R, Duan L M, Jaksch D, Cirac J I and Zoller P 2001 *Phys. Rev. Lett.* **87** 037901
[3] Amthor T, Reetz-Lamour M, Westermann S, Denskat J and Weidemüller M 2007 *Phys. Rev. Lett.* **98** 023004
[4] Heidemann R, Raitzsch U, Bendkowsky V, Butscher B, Löw R, Santos L and Pfau T 2007 *Phys. Rev. Lett.* **99** 163601
[5] Raitzsch U, Bendkowsky V, Heidemann R, Butscher B, Löw R and Pfau T 2008 *Phys. Rev. Lett.* **100** 013002
[6] Heidemann R, Raitzsch U, Bendkowsky V, Butscher B, Löw R and Pfau T 2008 *Phys. Rev. Lett.* **100** 033601
[7] Tong D, Farooqi S M, Stanojevic J, Krishnan S, Zhang Y P, Côté R, Eyler E E and Gould P L 2004 *Phys. Rev. Lett.* **93** 063001
[8] Jaksch D, Cirac J I, Zoller P, Rolston S L, Côté R and Lukin M D 2000 *Phys. Rev. Lett.* **85** 2208
[9] Mülken O, Blumen A, Amthor T, Giese Ch, Reetz-Lamour M and Weidemüller M 2007 *Phys. Rev. Lett.* **99** 090601
[10] Olaya-Castro A, Lee Ch F, Olsen F F and Johnson N F 2008 arXiv:0708.1159
[11] Sener M and Schulten K 2005 *Energy Harvesting Materials* ed D L Andrews (Singapore: World Scientific)
[12] Leibfried D, Blatt R, Monroe C and Wineland D 2003 *Rev. Mod. Phys.* **75** 281
[13] Blümel R, Chen J M, Peik E, Quint W, Schleich W, Shen Y R and Walther H 1988 *Nature* **334** 309
[14] Itano W M, Bollinger J J, Tan J N, Jelenkovic B, Huang X-P and Wineland D J 1998 *Science* **279** 686
[15] James D F V 1998 *Appl. Phys.* B **66** 181
[16] Porras D and Cirac J I 2004 *Phys. Rev. Lett.* **92** 207901
[17] Deng X-L, Porras D and Cirac J I 2005 *Phys. Rev.* A **72** 063407
[18] Lesanovsky I and Schmelcher P 2005 *Phys. Rev. Lett.* **95** 053001
[19] Hezel B, Lesanovsky I and Schmelcher P 2006 *Phys. Rev. Lett.* **97** 223001
[20] Djerad M T 1991 *J. Physique.* II **1** 1
[21] Cook R J, Shankland D G and Wells A L 1985 *Phys. Rev.* A **31** 564
[22] Büchler H P, Micheli A and Zoller P 2007 *Nat. Phys.* **3** 726
[23] Roos C F, Monz T, Kim K, Riebe M, Häffner H, James D F V and Blatt R 2008 *Phys. Rev.* A **77** 040302
[24] Auerbach A 1998 *Interacting Electrons and Quantum Magnetism* (Berlin: Springer)
[25] Calarco T, Cirac J I and Zoller P 2001 *Phys. Rev.* A **63** 062304
[26] Friedenauer A, Schmitz H, Glückert J T, Porras D and Schätz T 2008 arXiv:0802.4072
[27] Bloch I, Dalibard J and Zwerger W 2007 arXiv:0704.3011
[28] Lewenstein M, Sanpera A, Ahufinger V, Damski B, Sen De A and Sen U 2007 *Adv. Phys.* **56** 243
[29] Anderlini M, Lee P J, Brown B L, Sebby-Strabley J, Phillips W D and Porto J V 2007 *Nature* **448** 452
[30] Trotzky S, Cheinet P, Fölling S, Feld M, Schnorrberger U, Rey A M, Polkovnikov A, Demler E A, Lukin M D and Bloch I 2008 *Science* **319** 295
[31] Kitaev A 2006 *Ann. Phys.* **321** 2
[32] Micheli A, Brennen G and Zoller P 2006 *Nat. Phys.* **2** 341
[33] Brennen G K, Micheli A and Zoller P 2007 *New J. Phys.* **9** 138
[34] 2004 Special issue: Ultracold Polar Molecules: Formation and Collisions *Eur. Phys. J.* D **31**

[35] Roos C F, Lancaster G P T, Riebe M, Häffner H, Hänsel W, Gulde S, Becher C, Eschner J, Schmidt-Kaler F and Blatt R 2004 *Phys. Rev. Lett.* **92** 220402
[36] Nelson K D, Li X and Weiss D S 2007 *Nat. Phys.* **3** 556
[37] Gorshkov A V, Jiang L, Greiner M, Zoller P and Lukin M D 2008 *Phys. Rev. Lett.* **100** 093005
[38] Porras D, Marquardt F, von Delft J and Cirac J I 2007 arXiv:0710.5145
[39] Bose S 2003 *Phys. Rev. Lett.* **91** 207901
[40] Bose S 2007 *Contemp. Phys.* **48** 13
[41] Benjamin S C and Bose S 2003 *Phys. Rev. Lett.* **90** 247901
[42] Lee C F and Johnson N F 2004 *Phys. Rev.* A **70** 052322
[43] Burgarth D 2007 *Eur. Phys. J. Special Topics* **151** 147
[44] De Chiara G, Rossini D, Montangero S and Fazio R 2005 *Phys. Rev.* A **72** 012323
[45] Burgarth D and Bose S 2005 *New J. Phys.* **7** 135
[46] Burrell C K and Osborne T J 2007 *Phys. Rev. Lett.* **99** 167201
[47] Hoyos J A and Rigolin G 2006 *Phys. Rev.* A **74** 062324
[48] Allcock J and Linden N 2008 arXiv:0801.4867
[49] Rossini D, Giovannetti V and Fazio R 2007 *Int. J. Quantum Inf.* **5** 439
[50] Apollaro T J G and Plastina F 2006 *Phys. Rev.* A **74** 062316
[51] http://physics.nist.gov/PhysRefData/Handbook/periodictable.htm
[52] Cirac J I and Zoller P 1995 *Phys. Rev. Lett.* **74** 4091
[53] Schmidt-Kaler F, Häffner H, Riebe M, Gulde S, Lancaster G P T, Deuschle T, Becher C, Roos C F, Eschner J and Blatt R 2003 *Nature* **422** 408
[54] Monz T, Kim K, Hänsel W, Riebe M, Villar A, Schindler P, Chwalla M, Hennrich M and Blatt R 2008 arXiv:0804.0082v1
[55] García-Ripoll J J, Zoller P and Cirac J I 2005 *Phys. Rev. Lett.* **91** 157901
García-Ripoll J J, Zoller P and Cirac J I 2005 *Phys. Rev.* A **71** 062309
[56] Moller D, Madsen L B and Molmer K 2008 arXiv:0802.3631
[57] Nielsen M A and Chuang I L 2000 *Quantum Computation and Quantum Information* (Cambridge: Cambridge University Press)
[58] Schmidt-Kaler F, Eschner J, Morigi G, Roos C F, Leibfried D, Mundt A and Blatt R 2001 *Appl. Phys.* B **73** 807
[59] Pillet P, Smith W W, Kachru R, Tran N H and Gallagher T F 1983 *Phys. Rev.* A **37** 1527
[60] Stoneman R C, Thomson D S and Gallagher T F 1988 *Phys. Rev. Lett.* **50** 1042
[61] Seng M, Eichmann U, Lange V, Gallagher T F and Sandner W 1998 *Eur. Phys. J.* D **3** 21
[62] Czycholl G 2004 *Theoretische Festkörperphysik* (Berlin: Springer)